THE IMPACT OF EXTERNAL AND SELF-INDUCED MAGNETIC FIELDS

ON THE DEVELOPMENT OF CORROSION ON FEROUS

AND NON-FERROUS MATERIALS

by

CLINT G. GNEGY-DAVIDSON

Presented to the Faculty of the Graduate School of

The University of Texas at Arlington in Partial Fulfillment

of the Requirements

for the Degree of

DOCTOR OF PHILOSOPHY

THE UNIVERSITY OF TEXAS AT ARLINGTON

Summer 2016

ii

Acknowledgements

I would like to start off by thanking my family who encouraged and supported me throughout my academic years. The support of my fiancée, Ashley Hammer, my parents, Cindy, David, and Velina, have made getting through the multiple years of college less stressful.

I would also like to thank my advisor, Dr. David Wetz, for the several years of advice, mentorship, and friendship. Without his support I would not be in this position to receive this degree. I would also like to thank my committee members Greg Turner, Wei-Jen Lee, Ali Davoudi, and Rasool Kenarangui for their advice and support throughout the work of this dissertation.

I want to end by thanking my school mates and now friends Isaac, Chris, Derek, Matt, Caroline, Donald, Brian, Calvin, Kendal, Simon, Anthony, and Travis, for lending a helping hand, cultivating ideas, and making some great memories through the last few years. Without you all the past few years would have been a lot duller.

All of you have supported me throughout the years in getting this degree and finally the reward of graduating has come. Without all your help I would have not made it this far. Thank you all so much!

September 8, 2016

Abstract

THE IMPACT OF EXTERNAL AND SELF-INDUCED MAGNETIC FIELDS

ON THE DEVELOPMENT OF CORROSION ON FEROUS

AND NON-FERROUS MATERIALS

Clint Gnegy-Davidson, PhD

The University of Texas at Arlington, 2016

Supervising Professor: David Wetz

As the US Navy continues to field ships with an increasing number of electrical generators and loads, it is unclear how the high magnetic fields being generated throughout the ship will affect the corrosion rate of the ships structural and high current conducting alloys. Given the high-pulsed current carried by pulsed power systems, it is of increased interest to understand what impact their deployment will have on metallic corrosion. In this work, a number of experiments have been designed and performed to study these phenomena. In the first set of experiments several alloys have been subjected to a continuous, externally applied magnetic field while submersed in a 3.5% NaCl solution with and without

the presence of dissolved oxygen. In those without dissolved oxygen, argon is used to displace oxygen from the solution in order to determine the effect that oxygen has on corrosion. Within the subset of alloys being studied are ones with and without magnetic properties of their own that affect the distribution of magnetic flux around the sample when magnetic fields are present. A novel test stand was designed for the second set of experiments in which high pulsed currents, with amplitudes as high as a few kA, were conducted through 6.1 mm diameter rod samples. These experiments are aimed at studying how self-induced magnetic fields affect the rate of metallic corrosion of the same four materials evaluated in the first test series. Finally, a third test series has been performed in which samples have been subjected to repetitive pulsed current carry over a ten-minute period. In all experiments, diagnostic techniques including open circuit potential (OCP) measurements, anodic polarization measurements, linear polarization measurements, energy dispersive x-ray spectroscopy (EDS), and scanning electron microscope (SEM) imaging have been used to characterize each sample's corrosion properties with and without the presence of a magnetic field.

Table of Contents

List of Illustrations

x

List of Tables

Chapter 1

Introduction

Corrosion is a chemical reaction defined as the degradation of a material as it trends toward equilibrium within its environment. When a corrosion reaction occurs, a refined metal is converted to a more stable form and most of the time; a metal is oxidized by a reaction with the oxygen present in the system. Oxygen is often described as the 'fuel' for corrosion meaning that a reduction in oxygen content severely reduces a system's rate of corrosion [1] [2]. As will be shown in the work performed here, the presence of a magnetic field affects the concentration of oxygen within the system and therefore changes the rate of metallic corrosion. The reason for this is a result of oxygen's paramagnetic nature, which means that when oxygen is exposed to an external magnetic field it will induce its own internal magnetic field that is oriented in the same direction as the external field. This behavior causes the concentration of oxygen dissolved within the electrolyte to shift along the metallic surface depending on the magnitude of the magnetic field that is either applied externally or self-induced by high current flow through the metal. A shift in the oxygen concentration locally impacts the rate of corrosion or passivation, depending upon the material's corrosive properties. Early on

14

in this work, it was hypothesized that in the presence of magnetic field, the corrosion reactions are affected by reducing the concentration of oxygen at the surface of the sample. This report will document the experiments performed to validate this hypothesis.

Since the majority of the U.S. Navy's assets are located in salt-water environments that severely accelerate a metal's corrosion rate, they are a major investor in corrosion prevention research. In order to prevent the damage caused by corrosion, it is critical that the US Navy identify any mechanisms that affect metallic corrosion and they must identify new ways to inhibit the corrosion of its ships and ports. As the U.S. Navy advances the technology aboard its vessels, larger amounts of power will be required to run all of their essential electrical loads. Future electrical loads will vary anywhere from communications systems all the way to high-energy weapon systems. The ship leading the revolution with an all-electric platform is the Zumwalt class destroyer [3], which has two diesel generators that provide power for the entire ship including two electric propulsion motors. In addition to electric propulsion, there are a number of other advanced electrical loads planned for deployment aboard the Zumwalt class of destroyers. Many will have unique, high-power, transiently operated load profiles. Figure 1-1 displays many of the different electrical systems that will be aboard a Zumwalt class destroyer. A few of

the systems require that power be supplied at power levels in excess of

10s of MegaWatts either continuously or in a repetitive mode of pulsed

operation. Under these types of profiles, it is obvious that large amounts of

energy must be transferred throughout the ship. Voltage levels as high as

several kV and currents as high as several MA will be required. The

pulsed loads may require pulsed power sources capable of generating

short pulses ranging anywhere from 10s of picoseconds up to 10s of

seconds.
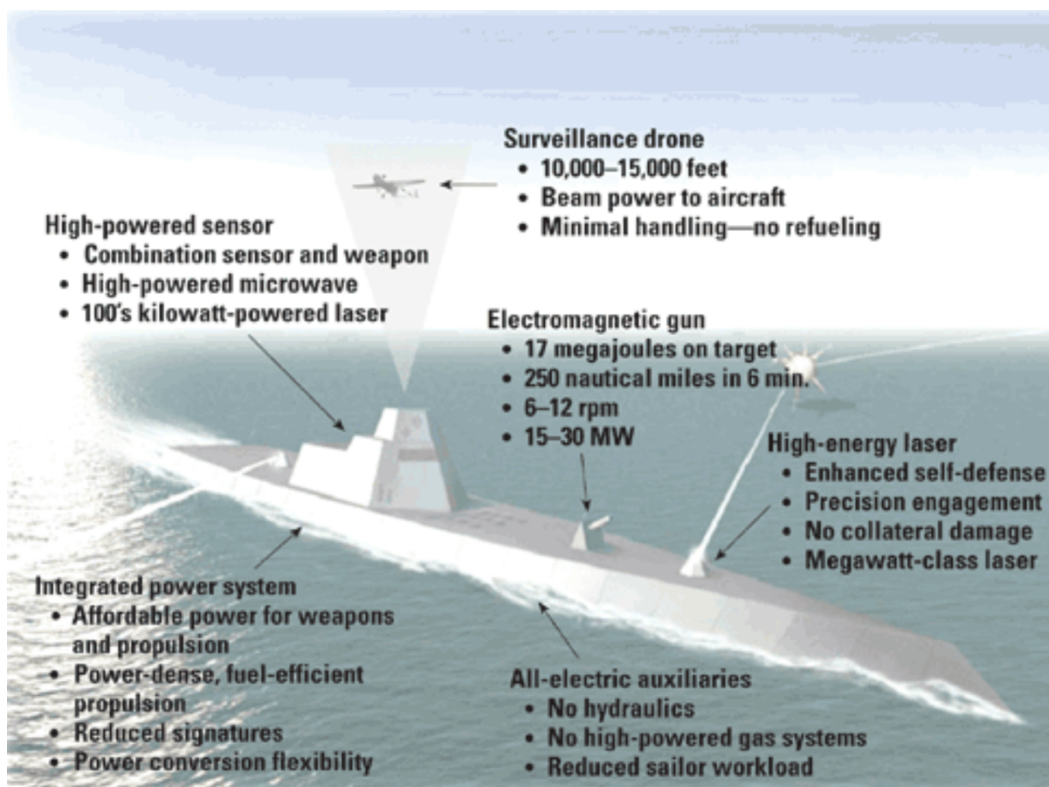
Figure 1-1 Electrical systems onboard the new Zumwalt class destroyer [3]

Large diameter electrical cables that line the hull of the ship will be used to carry power to all of the ship's electrical systems. As these cables carry high currents throughout the ship, very high magnetic fields are generated according to Biot-Savart law shown in equation 1.

$$B = \frac{\mu_o I}{2\pi r}$$ (1)

As shown in Equation 1, the strength of the magnetic field decreases as distance increases away from the wire however when high magnetic fields are generated, the objects in close proximity to them are exposed to significant field strengths [4] [5]. Materials in close proximity to the cables will vary considerably, ranging from copper alloys and aluminum alloys used in most electrical connections to carbon steel alloys, stainless steel alloys, nickel alloys, and titanium alloys, among others, that will be used in structural elements. Each of these different alloys has unique magnetic properties. An alloy with ferro-magnetic properties will concentrate the magnetic field lines, increasing the magnetic field local to the metal part considerably. Alloys that have ferro-magnetic properties often include one of the three elements: iron, cobalt, or nickel. As the navy begins to deploy these Zumwalt vessels and operate loads that generate high magnetic fields, it remains unclear how differently the electrical conductors and structural materials that are exposed to a magnetic field will corrode. The work performed here has been aimed at understanding

how magnetic fields affect metallic corrosion. A primary goal of the work

presented here has been to understand how the conduction of high-pulsed

electrical current through a metallic alloy, and the magnetic fields induced

by them, affects the rate of metallic corrosion. In the next section, a

background literature survey will be presented and in the sections that

follow, experimental processes will be discussed and the results obtained

will be presented.

Chapter 2 Background

Electromagnetism is defined as the interaction of electrically charged particles. Electrochemistry is a branch of chemistry that deals with the relations between electrical and chemical phenomena. Corrosion is defined as a chemical reaction in which a material gives up electrons in order to reach an equilibrium state. This dissertation combines several concepts from electromagnetic, electrochemical, and corrosion theories to understand the impact that each have on each other under unique circumstances. Though they are all interrelated, it may be difficult at first consideration to conceptualize how phenomena from each theory can affect the others. The section that follows will break down each of these concepts.

Magnetism

Magnetism is a physical phenomenon that results from the motion of electrical charge. Early investigations into magnetism were completed by an Englishman named William Gilbert in the late 16th century. Quantitative studies of magnetic fields did not begin until the late 18th century by a Frenchman named Charles Coulomb who defined the inverse square law of force. Knowledge of magnetism has advanced tremendously since the early days of discovery, but the sturdy foundation

was laid by these early researchers. There are several forms of magnetism, which include diamagnetism, ferromagnetism, and paramagnetism [6].

Materials that experience diamagnetism create a magnetic field in the opposite direction of an applied external magnetic field. Materials with these properties have a magnetic permeability less than μ_0. In most cases the effect of diamagnetism is very weak and in only a very few cases can the effect be visually seen. Because of the weak magnetic force, it is often thought that these materials are non-magnetic. Some common diamagnetic materials include: silver, lead, copper, carbon, and water [7].

Ferromagnetism is the strongest type of magnetism and is the mechanism behind the attraction of metals to magnets as well as the formation of permanent magnets. Ferromagnetism is often the only form of magnetism in which the force that is produced can be felt. When an external magnetic field is exposed to a ferromagnetic material, magnetic dipoles within the material's grain structure line up producing its own magnetic field in the same direction as the external field. When the external magnetic field is removed, the self-induced magnetic field remains. The most common ferromagnetic materials are iron, nickel, and cobalt. Nearly all alloys that are manufactured with high percentages of any of these elements are ferromagnetic [7].

Materials that experience paramagnetism form an internal induced magnetic field that is orientated in the same direction as an externally applied magnetic field. Most chemical elements are paramagnetic, including oxygen. Materials that are paramagnetic have a small susceptibility to magnetic fields and often require very high magnetic fields for the effect to be observed. Unlike ferromagnetic materials, paramagnetic materials do not retain any magnetization when the presence of an external magnetic field is removed. This is a result of the spin orientation being randomized, thereby removing any lasting magnetization effect [7].

Electromagnetics

In the early 19th century it was believed that magnetism and electricity were two different forces. James Maxwell changed this thinking with the publication of '*A Treatise on Electricity and Magnetism'* [8]. In that paper he presented results showing that positive and negative charges are controlled by the same force proving that there is a relationship between magnetism and electricity.

The electromagnetic force is known as one of the four fundamental forces [9]. The other fundamental forces include: gravitational, strong nuclear, and the weak nuclear force. These forces are interactions that occur in physical systems and have currently not been proven to be result

of a more basic interaction. The forces between two electrically charged

particles is known as electromagnetism. This interaction results in a

number of physical and fundamental phenomena, a few of which are a

focus in this dissertation. The first effect is the induction of a magnetic field

around a wire carrying current. The direction of the magnetic field is purely

dependent on the direction of the current flow and is often visualized with

the use of the right hand rule as seen in Figure 2-1.
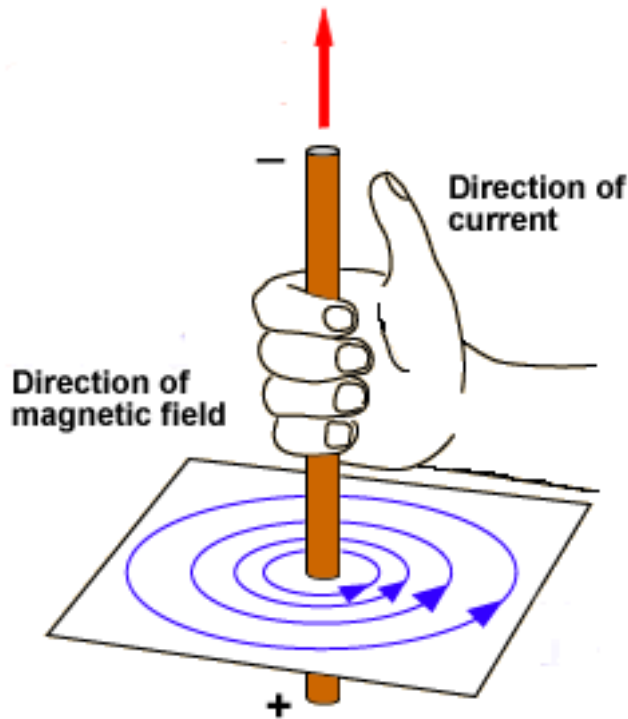
Figure 2-1 Diagram showing the use of the right hand rule [10]

The rule works by pointing the thumb in the direction of current flow and

wrapping the fingers around the wire. The direction of the fingers is the

same direction as the magnetic field. The second effect is observed as the

force between two charge particles decrease as the distance between the two particles increase. The force between the two particles as a function of distance is known as the inverse square law. In simple terms, the force tapers off quickly as the distance between the two particles increase.

In the experiments performed here, magnetic fields are being generated in a couple of different ways. In the first sets of experiments that will be presented, continuous magnetic fields are generated using an electromagnet. Simply put, an electromagnet is a big loop of wire wrapped around an iron core that concentrates the magnetic flux generated when current is passed through the wire. So that a uniform magnetic field is generated within the experimental working area, electromagnets often have two poles situated 180 degrees apart from each other, on either side of the working area. The strength of the magnetic field is a result of both the current through the windings as well as the distance between the poles. In the second set of experiments, magnetic fields are self-induced by flowing high pulsed current through the samples of interest. According to the right hand rule, a magnetic field is generated axially around the wire with field strength dropping off as a function of the distance away from the center. In the work being documented here, the affect these magnetic fields have on the paramagnetic properties of the environment are being studied. More about these details will be discussed later.

Corrosion

Corrosion is the chemical process in which a material losses ions in order to reach a more stable form, usually in the form of an oxide. Many people associate corrosion with rust. While rust is a form of corrosion, corrosion encompasses much more than rust. Rust is the term given to the orange iron oxide seen that develops when iron corrodes over time [11]. Rust is often seen on any iron surface that is exposed over time to the harsh environment such as older cars for example. Rust occurs when an iron-based alloy is exposed to an electrolyte, initiating the process of galvanic corrosion. When iron is in contact with a dissimilar metal and an electrolyte, electrons are releases into the electrolyte. At the same time, iron ions are released into the electrolyte which begin to bond with dissolved oxygen to form iron oxide, i.e. rust. Galvanic corrosion and pitting corrosion will be discussed here.

Galvanic corrosion is an electrochemical process that results from two separate reactions known as oxidation and reduction [12]. Galvanic corrosion occurs when two dissimilar metals are in electrical contact through an electrolyte solution. Oxidation is the anodic reaction that occurs on the electrode that has the lower potential within the galvanic cell. Corrosion damage occurs at the site of the anodic reaction. Reduction is the cathodic reaction that occurs on the electrode with the

higher potential within the galvanic cell. This electrode is protected within

the solution. Figure 2-2 presents the activity series in the order with an

increasing ease of oxidation going from bottom to top. As an example, if

zinc and copper were electrically connected and immersed in a solution,

zinc would begin to oxidize and copper would begin to reduce. This can be

determined by evaluating the table in Figure 2-2 and comparing the

rankings of zinc and copper. Zinc has a higher rank than copper so it will

oxidize in this galvanic cell. The activity series is useful in make design

choices for structural longevity in a specific environment. Figure 2-3

presents a graphical demonstration of galvanic corrosion occurring in both

an iron and zinc galvanic cell, shown on the left, and an iron and copper

galvanic cell, shown on the right. In the leftmost image, it is shown that

when the metals are electrically connected and immersed in solution, the

zinc begins to corrode as expected since it is higher on the activity series

than iron. As electrons begin to move from zinc to iron, zinc ions are

released into the solution that react with dissolved oxygen to form zinc

oxide. In the copper-iron galvanic couple, the iron begins to corrode since

it is higher on the activity series than copper. The iron ions that are

released react with dissolved oxygen to form iron oxide.

Metal	Oxidation Reaction
Lithium	$Li \rightarrow Li^+ + e\text{-}$
Potassium	$K \rightarrow K^+ + e\text{-}$
Barium	$Ba \rightarrow Ba^{2+} + 2e\text{-}$
Calcium	$Ca \rightarrow Ca^{2+} + 2e\text{-}$
Sodium	$Na \rightarrow Na^+ + e\text{-}$
Magnesium	$Mg \rightarrow Mg^{2+} + 2e\text{-}$
Aluminum	$Al \rightarrow Al^{3+} + 3e\text{-}$
Zinc	$Zn \rightarrow Zn^{2+} + 2e\text{-}$
Chromium	$Cr \rightarrow Cr^{3+} + 3e\text{-}$
Iron	$Fe \rightarrow Fe^{2+} + 2e\text{-}$
Cobalt	$Co \rightarrow Co^{2+} + 2e\text{-}$
Nickel	$Ni \rightarrow Ni^{2+} + 2e\text{-}$
Tin	$Sn \rightarrow Sn^{2+} + 2e\text{-}$
Lead	$Pb \rightarrow Pb^{2+} + 2e\text{-}$
Hydrogen	$H_2 \rightarrow 2H^+ + 2e\text{-}$
Copper	$Cu \rightarrow Cu^{2+} + 2e\text{-}$
Silver	$Ag \rightarrow Ag^+ + e\text{-}$
Mercury	$Hg \rightarrow Hg^{2+} + 2e\text{-}$
Platinum	$Pt \rightarrow Pt^{2+} + 2e\text{-}$
Gold	$Au \rightarrow Au^{3+} + 3e\text{-}$

Increase in Ease of Oxidation

Figure 2-2 The activity series for metals where the likeliness of corrosion to occur goes

up the list [13]
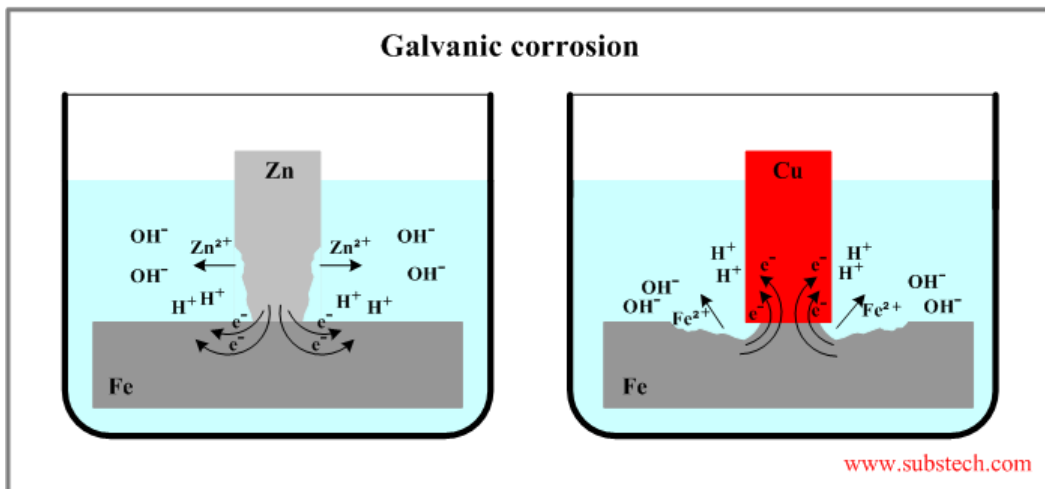
Figure 2-3 Galvanic corrosion occurring for zinc and iron on the left and copper and iron

on the right [14]

Engineered alloys composed of several different elements form their own unique galvanic cells. When the surface of an alloy is placed in contact with a solution, corrosion immediately begins to occur. As was described before, the element that is higher on the activity series is the one that will corrode. This can result in highly uniform or highly un-uniform corrosion of the alloy surface.

Pitting corrosion is a unique form of galvanic corrosion that is highly localized in the material. It can occur on any surface on which a protective oxide is formed. When two dissimilar metals are on in contact on the surface of an alloy, one area of the surface is cathodic in nature while another area is anodic. The chemical reaction that occurs causes pits to form on the surface of the alloy. Pitting can occur rapidly when the area of the cathodic surface is large with respect to the area of the anodic surface. The pitting continues as corrosion reactions occur causing them to become deeper. Often times an oxide will develop on the surface of the pit. Figure 2-4 shows the pitting process of stainless steel immersed in a sodium chloride solution. As electrons move to the more cathodic region, iron ions begin to corrode into the solution. This process repeats since there is a large cathodic area that forces the reactions to occur, deepening the pits. As the concentration of iron ions increases within the solution, iron oxide will begin to form on the surface of the pit, often hiding the

damage that was done to the metal. Pitting corrosion can be very detrimental to a material's structural integrity, while being difficult to identify. Since it is difficult to identify, electrochemical measurements are often needed to find and identify pitting corrosion. Scanning electron microscopes (SEMs) are often used to observe pitting on a microscopic level.
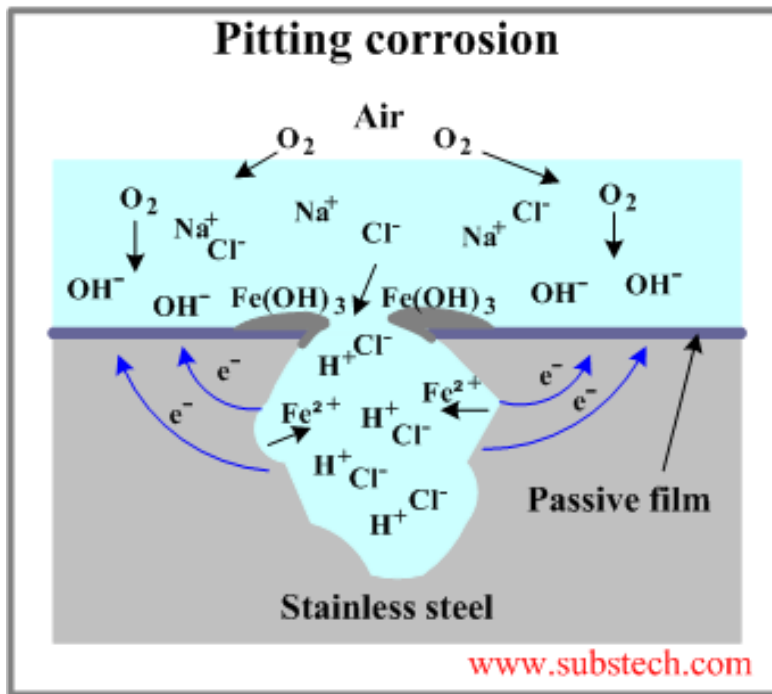
Figure 2-4 Pitting corrosion of stainless steel in a sodium chlorine solution [15]

Corrosion Analysis and Characterization Techniques

In the work performed here, a few different experimental techniques and procedures were used to study the impact of magnetic fields on the corrosion properties of metallic alloys. The electrochemical measurement

techniques used include: open circuit potential (OCP), anodic polarization (AP), and linear polarization resistance (LPR). The material characterization techniques utilized include: scanning electron microscopes (SEMs) and energy-dispersive X-ray spectroscopy (EDS). These different measurements and techniques will be discussed in more detail here.

Three-electrode electrochemical cells are used in the research performed here. As the name suggests, the cell has three different electrodes, namely the counter electrode, the reference electrode, and the working electrode, that are utilized. A graphical representation of a three-electrode setup is shown in Figure 2-5. The working electrode is the one being corroded and studied. The counter electrode is fabricated from a material that is lower on the activity series than the working electrode so that corrosion reactions are forced on the working electrode. The counter electrode is often made of graphite or platinum. It is important that the surface area of the counter electrode be at least twice that of the working electrode so that the reduction reaction is prevented from being a limiting factor. The third electrode is referred to as the reference electrode and it is used to prevent any current flow from affecting the voltage measured in the cell. Because electrochemical voltage measurements are often made in the μV to mV range, the reference electrode voltage must be very

stable. One of the more stable and rugged reference electrode is the saturated calomel electrode (SCE). All the experiments completed in the dissertation research presented here made use of a SCE reference electrode and thus all measurements are made in reference to the SCE voltage of 0.244 V.
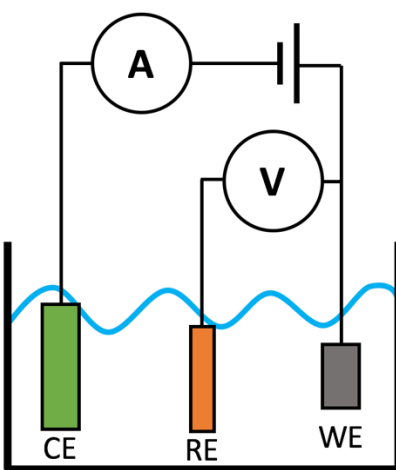
Figure 2-5 The three electrode setup with the connections made to a potentiostat. The green rectangle is the counter electrode, the orange rectangle is the reference electrode, and the grey rectangle is the working electrode

Figure 2-5 demonstrates the electrical connections made within an electrochemical cell. Voltage measurements are made between the working electrode and the reference electrode in order to prevent current flow from effecting the voltage measured. The current between the counter and working electrodes is most often measured. A power supply connected in series with the working and counter electrodes is used to

either source or sink current in the cell and can be used to control the galvanic cell's reactions.

Most electrochemical measurement techniques require that a three-electrode setup be used. One of the most basic measurement techniques is known as the open circuit potential (OCP) measurement. As its name suggests, it measures the open circuit electrochemical potential between the reference electrode and the working electrode. When a material is first submerged in a solution, oxidation and reduction reactions begin to occur. As the two reactions occur, the potential between these two electrodes changes, changing in the anodic or cathodic direction as time goes along. As the working electrode corrodes, it begins to trend to an equilibrium point where the anodic and cathodic reactions are equal and the change in the open circuit potential vs. time eventually settles below 0.1 mV/s. Once the voltage stabilizes, the cell has reached equilibrium and the stable potential measured is referred to as the corrosion potential. The OCP, or corrosion potential, is used as the starting point for future evaluations. When making this measurement, it is important that the potential is stable before beginning another experiment in the cell. If it is not stable, inaccurate results will be measured since the anodic and cathodic reactions are not equal. Once a stable corrosion potential is

measured, anodic polarization (AP) or linear polarization resistance (LP) measurements can be made.

Using the anodic polarization (AP) technique, the working electrode is polarized in the anodic direction across a range of potentials using an external power supply. Measurements made using this technique can be used to identify several corrosion properties of the sample under test. Sample results measured from an active-passive metal are displayed in a potential vs. logarithmic current plot in Figure 2-6. The plot shows the active, passive, and transpassive regions of an active-passive metal. The active region is where a metal will corrode and is the region where the corrosion current density is measured. As the applied potential increases, the current density begins to increases as the metal reaches the passive region. The passive region is the region where a passivation layer begins to develop on the surface of the sample. A decrease in current density results from the metal forming a protective passivation layer. Eventually the passivation layer will begin to breakdown as it reaches the transpassive region. It is in this region that pitting occurs and for that reason it is often referred to as the pitting region. As the passivation layer breaks down, small localized areas begin to corrode and this is when deep pits can develop. As discussed previously, pitting is very detrimental to a metals structural integrity. From the data in Figure 2-6, there are six

measurements that can be used to determine the corrosion properties of a
metal within an aqueous solution.
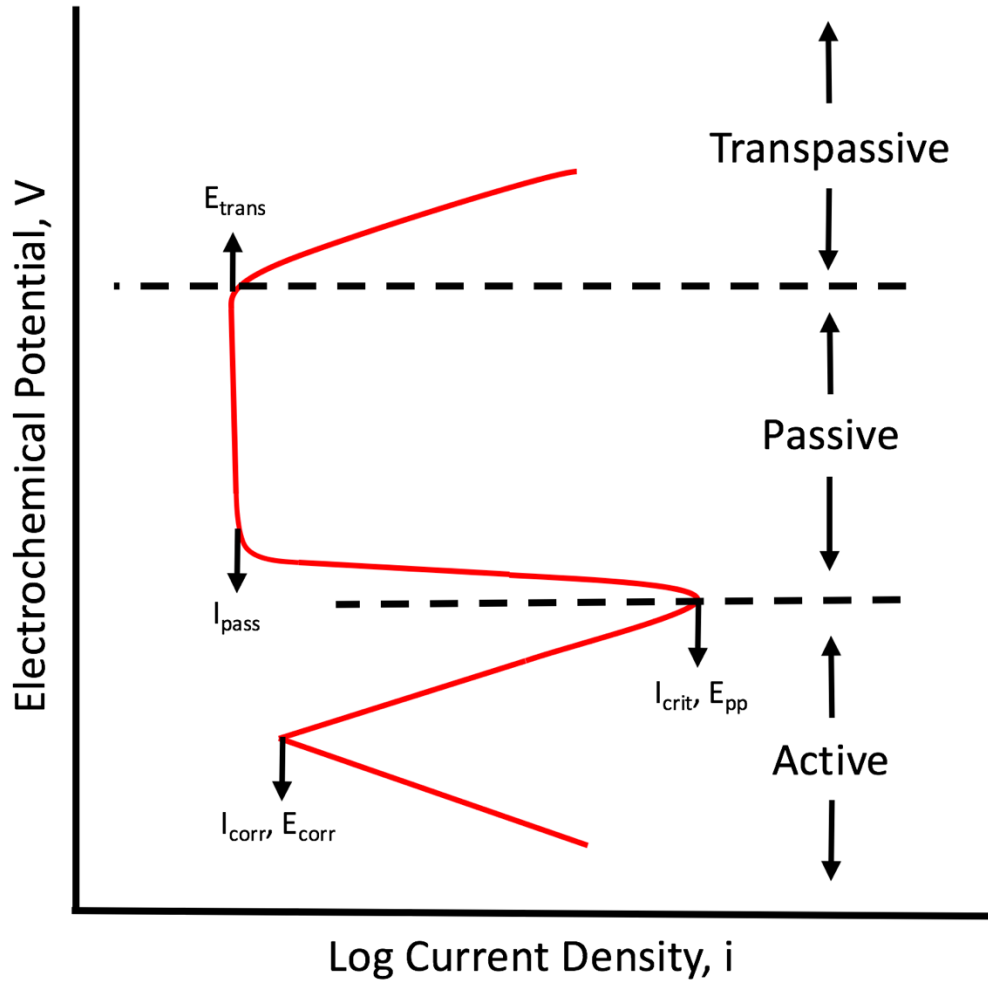
Figure 2-6 Anodic polarization plot of an active-passive metal

The six measurements include the transpassive potential (E_{trans}),
passivation current density (I_{pass}), critical current density (I_c), passivation
potential (E_{PP}), corrosion current density (I_{corr}), and corrosion potential
(E_{corr}). The transpassive potential is the point at which the metal will begin

to pit. The passivation current density gives insight on the rate of corrosion once the metal has passivated. The critical current density is the amount of current required to achieve the passivation potential. The passivation potential is the point at which the metal beings to passivate. The corrosion current density and the corrosion potential are measured when the metal is at equilibrium. All these measurements are useful in understanding and controlling how a metal will corrode in an aqueous solution.

The AP technique disrupts how a metal rests in the solution therefore, additional techniques need to be used if it is necessary not to affect the sample's surface. The linear polarization resistance (LPR) measurement is a common non-intrusive technique that is used to make measurements of a metal's corrosive tendency in a solution without altering the surface chemistry. The LPR measurement is normally very short in duration and it does not polarize the sample enough to alter the surface reactions. When making the measurement, the cell's potential is typically swept from -10 mV to 10mV vs. the OCP. Using the applied potential and the resulting current within the cell, the corrosion resistance can be calculated and used as a metric to compare how fast the sample will corrode in a specific electrolyte.

Several electrochemical methods can be used to explore the corrosion kinetics and thermodynamics of a material in a specific

environment but material characterization must be used to understand changes to the structure and properties of a sample's surface. By using scanning electron microscopes (SEMs) and energy dispersive X-ray spectroscopy (EDS) a surface can be studied in depth. Materials are often characterized by both methods to understand the type of corrosion and corrosion products.

A scanning electron microscope (SEM) is an electron microscope that uses a focused beam of electrons and the energy reflected from them to produce an image. A beam of electrons is emitted at the surface of a specimen. Once the electron hits the surface of the specimen it emits secondary electrons, which are then detected by a detector. By counting the number of electrons detected, an image can be constructed showing the change in depths on the surface. In corrosion research, the ability to see changes on the surface of the sample is helpful. SEM imaging can be especially helpful for measuring the pits formed in the pitting corrosion process.

Energy-dispersive X-ray spectroscopy (EDS) is used to perform environmental analysis of a sample. EDS systems are often integrated into an SEM such that SEM and EDS measurements can be made simultaneously. EDS works through the interaction of an X-ray excitation with the surface of a sample. An x-ray source excites an inner shell

electron causing it to be ejected from the sample leaving behind an electron hole. The hole is then filled with an electron from a shell of higher energy and the energy released is the form of an X-ray that is measured by a spectrometer. The energy released is specific to the element and therefore measurement of that energy enables the composition of the sample to be identified.

It is hoped that this discussion has provided good insight into the measurement techniques used in the analysis of corrosion. Each method describes in different ways how the alloy under study has been affected. Using the techniques listed above, the impact magnetic fields have on the corrosion of metallic alloys is being studied.

Corrosion and Magnetic Fields

The relationship between corrosion and magnetic fields has been previously studied but only briefly and not under the high pulsed conditions studied here. Oxygen is an element that drives the way in which magnetic fields impact metallic corrosion. Oxygen is paramagnetic in nature but in open air, it moves too fast to be affected by magnetic fields. Oxygen dissolved in an electrolyte solution moves much slower so it is affected by the application of an external magnetic field. The interaction affects corrosion properties by altering oxygen concentration at the surface of the corroding metal. Changes in the concentration of

oxygen alters the cathodic reaction affecting a variety of corrosion mechanisms. Next a literature survey will be presented documenting previous research performed investigating the relationships between magnetic fields and metallic corrosion.

Linhardt, et. al. investigated the impact a magnetic field has on the chloride induced pitting of stainless steel [16] [17] [18]. In his experiments, he used 304 stainless steel and an externally applied magnetic field with a peak value of 0.3 T. The magnetic field was induced using a permanent magnet that was oriented beneath a cylindrical sample. In his results, multiple phenomenon was observed. First, a vortical flow, induced by the magnetohydrodynamic effect (Lorentz force), was formed within the electrolyte when the magnet was present. The flow was formed when the ions in the solution were carried by the Lorentz force as they moved within the solution. The flow and the non-uniform flux density on the sample's surface induced changes in the pitting pattern and their depth on the stainless steel's surface. Without the magnetic field applied, large pits formed in a uniform distribution across the entire surface. On the other hand, when the magnetic field was applied, larger pits at a lower density were observed at the center of the sample while the pits along the edge of the sample were present at a higher density with a shallower depth. This is all shown graphically in Figure 2-7.
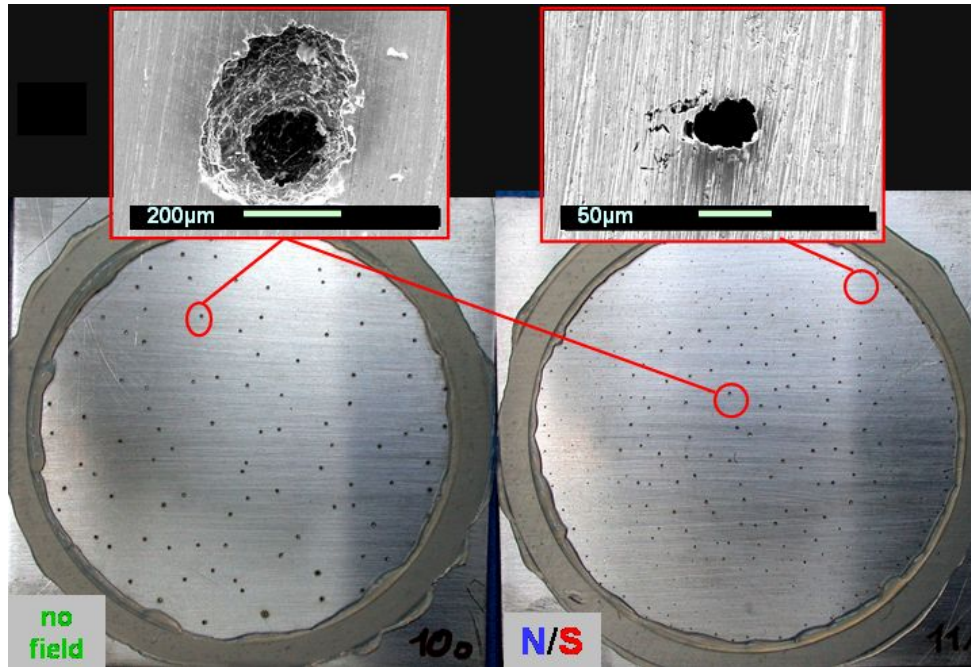
Figure 2-7 Pitting corrosion of 304 stainless steel with and without a 0.3 T magnetic field

[17]

Among the conclusions drawn from Linhardt, et. al. is that the change in

the pitting pattern may be attributed to the variation of the magnetic field's

strength and non-uniform density across the sample's radius. The field is

weaker, more uniform, and is essentially in line, parallel, with the natural

ion flow at the sample's center. The field is stronger and more divergent

along the sample's outer edge. Therefore, pitting at the center of the

sample appears similar with and without a magnetic field applied. Along

the sample's edge, the field lines are more divergent, creating a stronger

non-uniform field with a non-parallel orientation to the natural ion flow.

This results in the ions feeling a stronger Lorentz force that alters their

velocity and direction resulting in a different pitting pattern along the edges.

Sato, et al. experimented with high strength magnetic fields to understand its impact on corrosion formation in carbon steels [19]. Using a superconducting magnet, 10 T was applied to a cylindrical piece of carbon steel. While the magnetic field was applied, corrosion formed on the lateral surface of the cylinder, while the top and bottom of the cylinder had limited corrosion, if any at all. The corrosion patterns are shown in Figure 2-8.

(a) B=5T, 6h

(b) B=5T, 6h

(c) B=10T, 18h

(d) B=0T, 6h
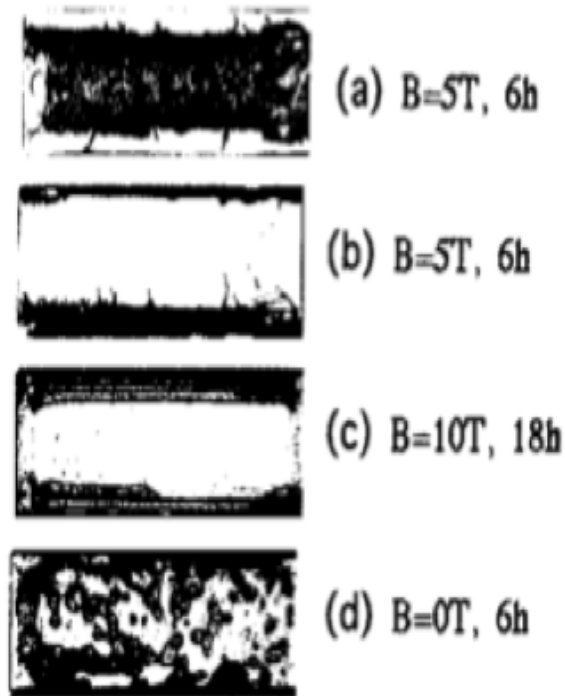
Figure 2-8 Corrosion patterns of steel cylinder on the (a) lateral surface (b), (c) upper surface, and (d) any surface [19]

Without the magnetic field applied, the corrosion formed uniformly on all sides of the steel cylinder. It is thought that the magnetic field influences the location of the dissolved oxygen thereby altering the location of corrosion. Oxygen is paramagnetic and therefore, attracts to where the magnetic fields are strongest on the steel sample. Sato used aerobic bacteria to determine if the oxygen concentration was highest where corrosion was occurring and to relate it to the movement of oxygen under influence of a magnetic field. The bacterium thrives in the higher concentration of oxygen, which can be used to determine where the highest oxygen concentration is on the surface of the steel. By allowing the bacterium to grow for a set period of time and then killing the bacteria quickly the amount of bacteria can be counted over the surface of the sample. The higher amount of bacteria indicates locations of higher oxygen concentration and in Sato's experiment it shows the higher oxygen concentration at the locations of corrosion and highest strength magnetic field. This finding indicated that the magnetic field influences the location of oxygen and alters the location of corrosion. No work was done to measure the actual corrosion potential or the corrosion kinetics of the tested alloy.

Ghabashy experimented on mild steel with an external magnetic field to determine the impact on corrosion rate [20]. Through his findings it

was determined that an increasing magnetic field strength would decrease

the corrosion rate of the mild steel. The results of his findings are shown in

Figure 2-9.
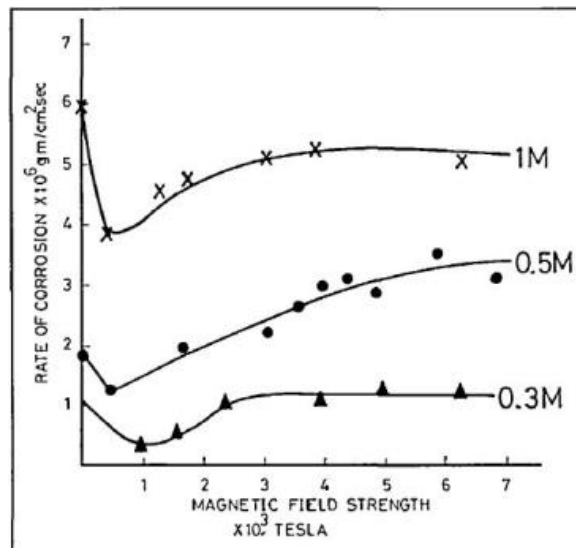
Figure 2-9 Rate of corrosion as a function of magnetic field strength and molarity of ferric

chloride

R. Pietrzak and R. Szatanik used positron annihilation to determine the

impact of magnetic fields on corrosion of iron and St20 steel [21]. Using

this method, they were able to investigate the very early stages of

corrosion and determined that magnetic fields reduced the creation of

corrosion-induced defects in iron and St20 steel. J. Hu et al. applied

magnetic fields to beryllium copper in a NaCl solution and measured the

changes in open circuit potential and current density [22]. It was found that

the corrosion potential shifted slightly, while the current density was

altered but was dependent on the concentration of NaCl. It was concluded that the magnetic field was accelerating the diffusion of $CuCl^2$ away from the sample and delayed the formation of the Cu_2O.

Various other researchers have done research on the effects of magnetic fields to water and dissolved oxygen. They explore the impact the magnetic field had on the movement of water as well as change in oxygen concentration [23] [24] [25] [26] [27]. More background information on the study of magnetic fields on the impact of corrosion can be obtained through various other articles [28] [29] [30] [31] [32] [33]. Though these researchers have laid groundwork for understanding how magnetic fields affect the corrosion of metallic alloys, their work stops short of addressing how high strength magnetic fields generated through the conduction of pulsed current through the sample, affect its rate of corrosion and the mechanisms that drive it. The work presented here adds their foundation with knowledge in this area.

Chapter 3 Experimental Setups

As discussed earlier, several unique experimental setups have been assembled to perform the work discussed here. The first setup studied several alloys of interest under the influence of a high strength continuous magnetic field. The second setup explored the impact high pulsed current carrying conductors effect corrosion properties. Because of the unique space constraints, custom three electrode test cells were constructed for electrochemical characterization and those will also be discussed.

External DC Magnetic Field Experimental Setup and Procedure

The work presented here is aimed at evaluating how a high strength magnetic field, 0.45 T, affects the corrosion potential of various ferrous and non-ferrous metallic alloys with varying compositions. While previous work, discussed earlier, has shown that magnetic fields do have an impact on the pitting patterns of metals, little is discussed of how and why the magnetic fields impact the corrosion behavior. So that these relationships can be better understood, a novel experimental setup was designed and fabricated. The electromagnet used to generate the magnetic field in the experiments created unique constraints on the test

43

cell. One constraint involves the requirement that the test cell had to fit tightly in between the two poles of an electromagnet. This made using a typical large commercial off the shelf (COTS) electrochemical test cell impossible, as the width of the COTS cells was wider than the free space. To overcome these challenges, a 1000 mL glass beaker was used and the air gap between the two electromagnet poles were placed as close as physically possible such that the magnetic field strength was roughly 0.45 T near the sample's surface. The 1000 mL was sufficient in providing enough separation between the working, reference, and counter electrodes, respectively. When OCP measurements were made, only reference and working electrodes were required but the same experimental setup was used, leaving the counter electrode in place for consistency with later experiments. A photograph of the electrochemical setup utilized is shown in Figure 3-1.
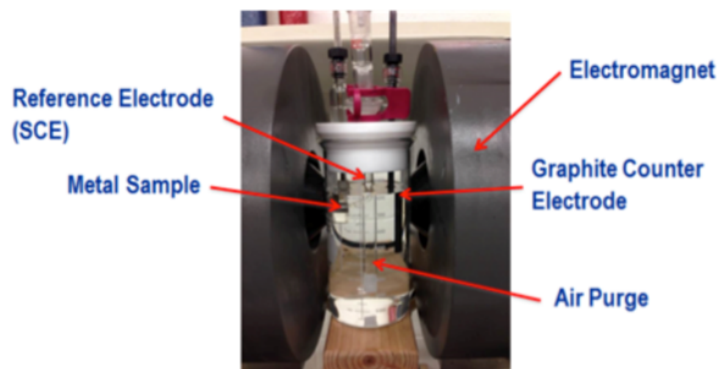
Figure 3-1 Electrochemical test cell located within a toroidal DC electromagnet

The orientation of the magnetic field relative to the sample is shown in Figure 3-2 where it should be noticed that the magnetic field is oriented perpendicular to the surface of the sample under test. A custom Polytetrafluoroethylene (PTFE) lid was fabricated to fit inside the 1000 mL beaker to hold the counter, working, and reference electrodes, respectively. A Princeton Applied Research saturated calomel electrode (SCE) was used as the reference electrode in all experiments. This electrode was chosen because of its ability to maintain a very stable potential as well as its ease of maintenance. The metal alloy under test acts as the working electrode in all experiments and the counter electrode being made of graphite. In some experiments, a purge tube was used to introduce gas that displaces oxygen from the beaker. The port through which the purge tube is place is also shown in Figure 3-1 and Figure 3-2 respectively.

1. Reference Electrode (Open Circuit Potential and Anodic Polarization)
2. Counter Electrode (Anodic Polarization)
3. Epoxied Sample (Open Circuit Potential and Anodic Polarization)
4. Argon Purge (Used only in argon experiments)
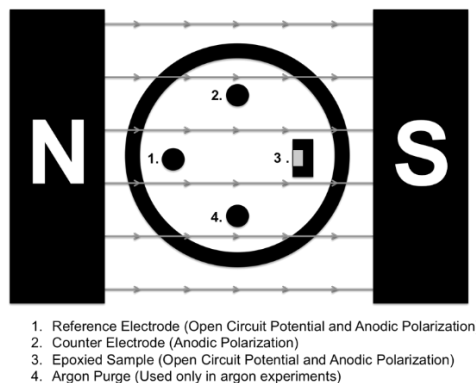
Figure 3-2 Orientation of the three electrodes with respect to the field lines of the electromagnet

During all of experiments in which the beakers were used, they were filled with 800 mL of 3.5% w.t. NaCl aqueous solution. Open circuit potential measurements were made to evaluate the metal's corrosion behavior both with and without a magnetic field applied. As discussed earlier, when an alloy is placed in an electrolyte, the number of anodic and cathodic reactions are limited. As the reactions take place, the open circuit potential changes until eventually there is a point where it stabilizes such that the change in potential is less than 0.1 mV/s. When stable the rate of cathodic and anodic reactions are equal. In these experiments, the corrosion potential was measured using a Princeton Applied Research Versastat 4 potentiostat. A Lake Shore EM4 electromagnet powered by a Lake Shore model 647 power supply was used to create a uniform DC magnetic field across the test cell. Using a LakeShore 450 gaussmeter and a magnetic field probe positioned on a horizontal axis, the magnetic field as a function of distance within the working area of the test cell was measured, shown in Figure 3-3. From Figure 3-3, it can be seen that the magnetic field strength at the surface of the working electrode is roughly 0.45 T.

It is important to remember that the magnetic field plotted in Figure 3-3 is not representative of what it is within the test cells when metals having different permeability are present. 2D-magnetic field simulations

were performed using a simple finite element solver for estimation of the magnetic field across the samples of interest.
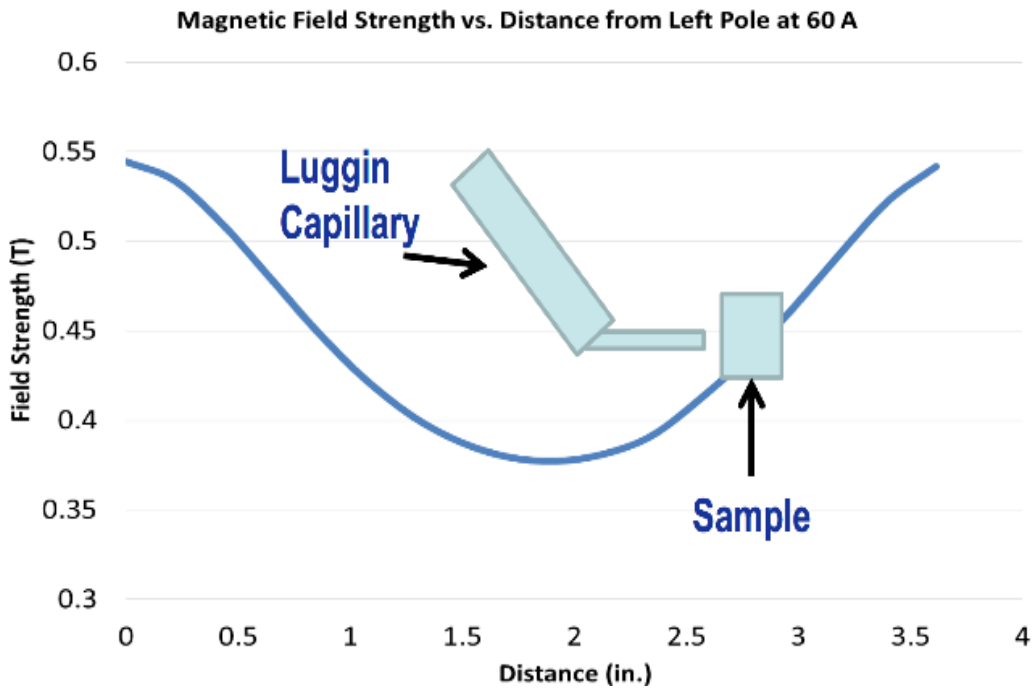
Figure 3-3 Plot of magnetic field strength vs. position when the electromagnet's field current is 70 ADC

It is important to remember that the magnetic field plotted in Figure 3-3 is not representative of what it is within the test cells when metals having different permeability are present. 2D-magnetic field simulations were performed using a simple finite element solver for estimation of the magnetic field across the samples of interest. As seen in Figure 3-4 a through d, the magnetic field across the surface of the working electrode varies considerably depending upon its ferrous properties. When

comparing the field lines of the four different samples, which incidentally

are four of the materials studied in this work, it is easy to notice how the

flux density is higher near the surfaces of the more permeable steels. The

flux is especially high near the outer perimeter of the sample.
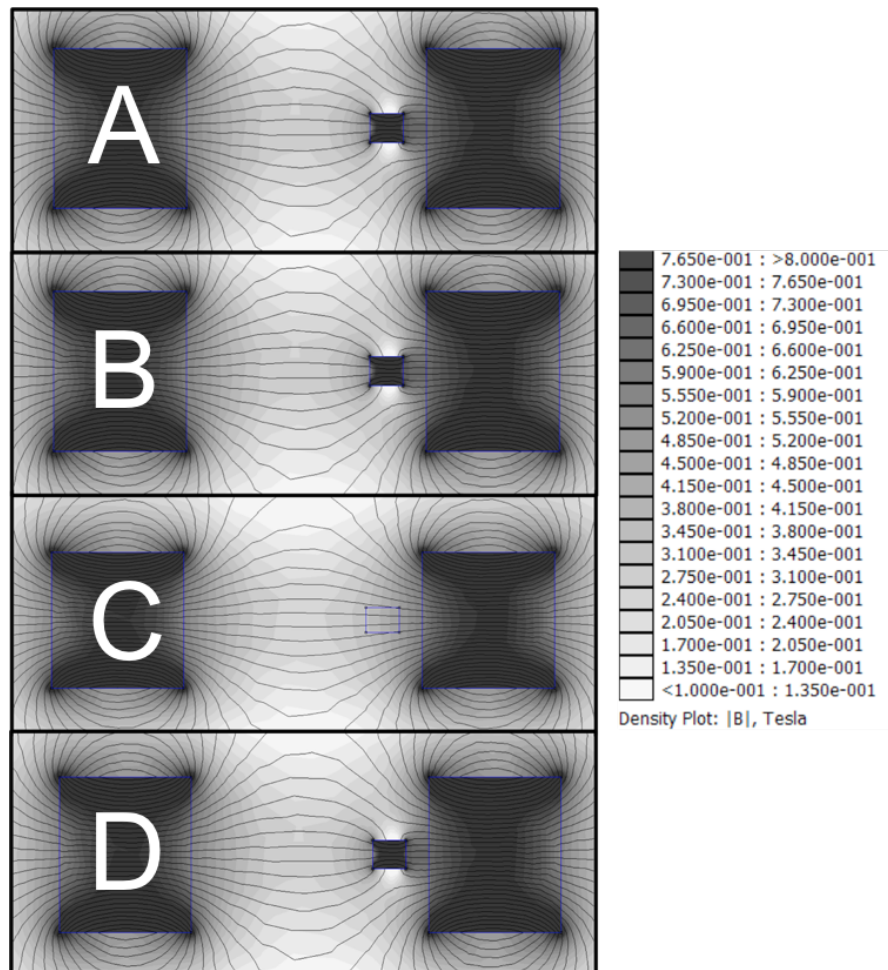
Figure 3-4 Magnetic simulations of the electromagnet setup demonstrating the impact of

the metals ferrous properties on the field lines and field strength across each alloys

surface: (a) 1018 steel, (b) 8620 steel, (c) 304 stainless steel, and (d) 416 stainless steel

The alloy compositions of the alloys tested here, 304 austenitic stainless steel, 416 stainless steel, 1018 steel, 8620 steel, Cu 110, Cu 182, Al 6061, and Al 7075 are documented in Table 1 through Table 3. Among these materials are a few with very high magnetic permeability while others are nearly equal to 1 enabling the impact of magnetic properties to be included in the research matrix. In the initial OCP experiments, only the 1018 steel, 8620 steel, 304 stainless steel, and 416 stainless steel alloys were evaluated. For all experiments two samples were made of each material to undergo testing. All samples were cut from 1 cm diameter rods of each material type and all rods of each respective material type were obtained from the same vendor and cut from the same stock. Once cut, one sample was used in the baseline experiments while a different, but identical sample, was used in experiments in which a magnetic field was present. Different samples were used to ensure consistency as well as to eliminate any impact from a residual magnetic field present in the materials after a magnetic field test was performed. The samples were experimentally used several times under identical test conditions in order to obtain statistical validation of the results. Each sample was re-polished between experiments to reset the material back to its initial condition before the next experiment was performed.

Table 1 Manufactured specifications of 304 stainless steel, 416 stainless steel, 1018 steel, and 8620 steel

	C (%)	Cr (%)	Fe (%)	Ni (%)	P (%)	Si (%)	S (%)
304 SS	0.42	22.41	66.01	9.48	0.05	0.57	0.57
416 SS	0.89	18.50	77.52	0.01	0.51	1.32	0.55
1018 Steel	0.43	0	96.64	0	0.01	0.83	0
8620 Steel	0.40	0.59	97.45	0.24	0.31	0.76	0

Table 2 Manufactured specifications of Cu 110 and Cu 182

	Cu (%)	O (%)	Cr (%)
Cu 110	99.9	0.04	0
Cu 182	99.1	0	0.9

Table 3 Manufactured specifications of Al 6061 and Al 7075

	Al (%)	Cu (%)	Fe (%)	Cr (%)	Mn (%)	Si (%)	Mg (%)	Ti (%)
Al 6061	96.9	0.25	0.7	0.25	0.15	0.6	1.0	0.15
Al 7075	93.86	2.0	0.5	0.24	0.3	0.4	2.5	0.2

Each sample was mounted in epoxy to ensure that a controlled exposure area with the electrolyte could be maintained. Once potted, they were rough ground and polished using a 1000 grit sand paper before finally being fine polished using a 0.1-micron alumina paste. Figure 3-5 contains a photograph of a typical 1018 steel sample after all polishing procedures were completed.

Figure 3-5 Polished 1018 steel sample

While corrosion potential measurements were being made, the

material under test was rested for three hours in 800 ml of room

temperature 3.5% NaCl solution. This amount of time was found to be

sufficient for all corrosion potentials to fully stabilize. Though it was not

monitored throughout each test, the temperature of the NaCl always

started out between $16^{o}C$ and $20^{o}C$ and there were no factors present that

should have ever elevated the temperature above standard room

temperature.

After each open circuit potential experiment was completed,

scanning electron microscope (SEM) images of the sample were taken for

comparison to those made prior to experimentation. A Hitachi S-3000N

Variable Pressure SEM was used. In the case of the stainless steels, the

images were taken at 1000x magnification with a 25 kV accelerating

voltage. In the cases of 1018 and 8620 steel, respectively, a zoom of 100x and 500x were used at a 25 kV accelerating voltage.

It was hypothesized prior to experimentation that the magnetic field would influence the oxygen concentration at the surface of the sample and alter the corrosion potential as well as the corrosion kinetics. To determine if oxygen is the main contributor, argon was used to displace oxygen in the test cell. In a separate set of identical experiments, the 1018 steel, 8620 steel, 304 stainless steel, and 416 stainless steel samples were submerged in a NaCl solution for six hours. As they did in the original experiments discussed, the test cell consisted of three electrodes, however it was in these experiments that the purge tube was added. Two experiments were completed using each of the materials studied, one in which the test cell was saturated with air and one in which it was saturated with argon. During the first three hours of each experiment, the magnetic field was left off and the corrosion potential was allowed to stabilize. After three hours had passed, the magnetic field was turned on and the experiment continued to rest for an additional three hours. These experiments confirmed that oxygen did in fact play a role in altering the corrosion potential of the test cell when a magnetic field was present.

In a final series of experiments, anodic polarization measurements were added to the test procedure. As in the previous experiments, the

corrosion potential was allowed to stabilize for three hours. After three hours had passed, the anodic polarization measurements were made. When making these measurements, the working electrode was anodically polarized by sweeping the potential from -20 mV to 700 mV versus the OCP. All eight alloys listed in Table 1 through 3 were studied with the additional materials added to give a broader perspective than just steels and stainless steels. As a reminder, the anodic polarization measurement is used to measure the corrosion current density, pitting current density, pitting potential, and transpassive potential.

Pulsed Current Experimental Setup and Procedure

In this second type of experiments, the aim of the research was to understand the impact of high-pulsed current flow and their self-induced magnetic fields on the corrosion rate of metallic alloys. A capacitive pulsed power supply was utilized, shown in Figure 3-6, to supply pulsed current through the sample under test that serves as the load. The configuration of the load is shown in Figure 3-7 and Figure 3-8. In Figure 3-7, it is shown how current flows through the sample and returns to the supply in two identical paths so that the electromagnetic forces are balanced.

The power supply is used to supply pulsed currents as high as ~10 kA through the samples being evaluated. The full-width-half-max (FWHM) length of the pulse is roughly 4 ms. The length of the pulse was selected

to replicate the FWHM length seen by loads of interest from the Navy. The power supply is made up of eighteen identical, but separate, capacitive power supplies, each of which is comprised of ten, 3.5 mF, 450 V capacitors connected in parallel. Each capacitive module has a 40 mH inductor used for pulse shaping and they are switched to the load using silicon controlled rectifiers (SCRs). Crowbar diodes are employed to prevent oscillation in the RLC circuit.
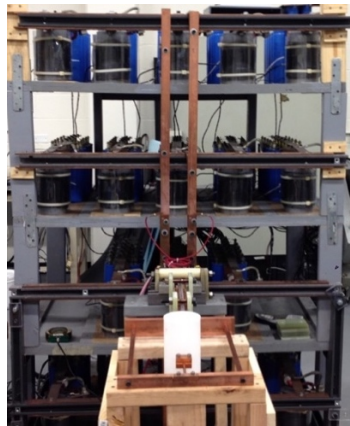
Figure 3-6 Pulsed power supply utilized to pulse high currents through the test samples being studied
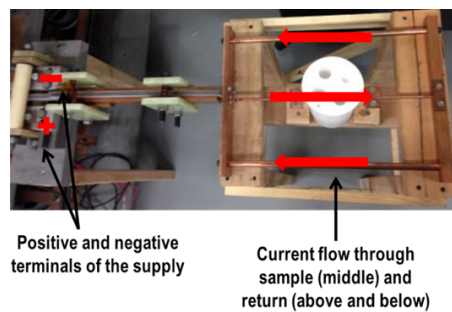
Figure 3-7 Electrical load made up of the test cell, rod sample, and high current bus work. The red arrows show the path of the current
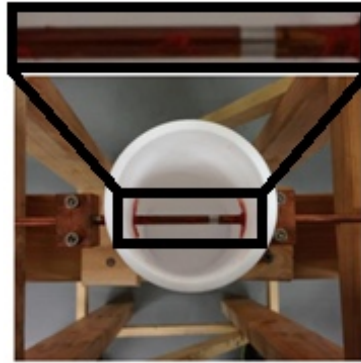
Figure 3-8 Photograph of a 304 stainless steel sample (top) housed within the test cell (bottom) containing the NaCl solution. Polyimide tape is used to limit the exposed surface area to 1cm^2

In these experiments, rod samples with a diameter of 6.35 mm were used so that the skin effect could be neglected. So that the exposed area could be limited to ~1 cm^2, the bulk of the sample was covered in polyimide tape. This is seen visually in Figure 3-8. The rod sample under test is passed through a custom PTFE beaker that holds 800 ml of 3.5% NaCl electrolyte. PTFE was used since it was machinable to allow the rod to pass through while remaining transparent to the magnetic fields. The sample is held within the load using copper saddle clamps. Since the electrolyte is liquid based, the experiments were designed so that the sample's surface temperature was held below 100°C, the boiling temperature of water. Rod samples were initially pulsed in an open-air environment with increasing currents and an insulated thermocouple mounted on the surface. From those experiments, the peak currents that

could be carried through the sample were determined such that they limit the surface temperature below 100°C.

Sample current pulses measured through each of the four materials evaluated, 1018 steel, 8620 steel, 304 stainless steel, and 416 stainless steel, respectively, are shown in Figure 3-9. The maximum current was roughly 8.7 kA through the 1018 steel sample. The 8620 steel sample was only slightly lower than that through the 1018 sample while the currents through the stainless steel samples were roughly 2 kA lower than those through the two respective steel samples. The high-pulsed current induces a magnetic field that wraps around the sample according to the right hand rule. Figure 3-10 plots simulated magnetic field contours of 1018 and 8620 steel simulated with a peak pulsed current flow of 9 kA. Figure 3-11 plots similar magnetic field contours when 304 and 416 stainless steel samples, respectively, are simulated with a peak pulsed current flow of 6 and 6.5 kA, respectively. As seen in the figures, the peak amplitudes measured are in excess of 3 T within all of the samples except for 304 stainless steel which peaks just over 0.5 T. This is expected since 304 stainless steel is the only sample that does not have a magnetic permeability higher than 1. From the figures it should also be noticed the magnetic field strengths at distances greater than the rod's surface drop off considerably and are all roughly equivalent.
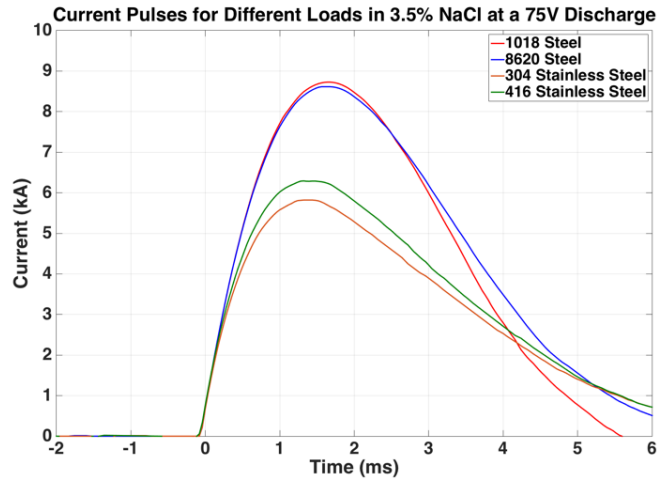
Figure 3-9 Samples of the pulsed currents sourced through each respective material

being evaluated here
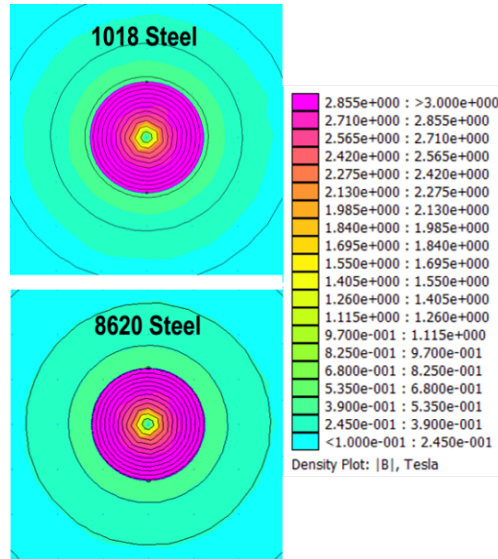
Figure 3-10 Simulations of the magnetic field, 1018 steel (top) and 8620 steel (bottom)

when pulsed with the currents applied here. The magnetic field simulations assume a

sinusoid with a frequency of 111 Hz is applied to the conductor
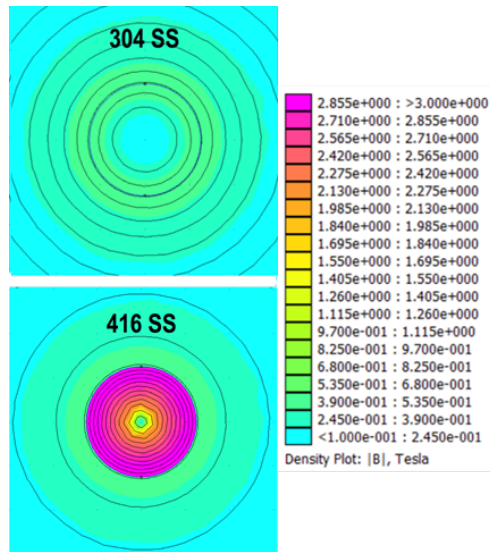
Figure 3-11 Simulations of the magnetic field, 304 stainless steel (top) and 416 stainless steel (bottom) when pulsed with the currents applied here. The same 111 Hz signal is being applied as in Figure 3-10

With each rod material evaluated here, two sets of experiments were performed. In the first, the samples material's surface properties are characterized, next they are exposed to electrolyte for three hours at room temperature, linear polarization measurements were made, and finally they are characterized again. This experiment serves as a baseline for measuring the material's corrosion rate due to electrolyte exposure alone. In the second set of experiments, the samples surface properties are characterized, the rods are pulsed with current nineteen times over a three-hour period while immersed in electrolyte at room temperature, linear polarization measurements are made, and finally the materials

surface properties are characterized a final time. The shot rate of nineteen shots over a three-hour period sets a rep-rate of one shot every ten minutes. It should be noted that the samples used in each type of experiment cut from the same base alloy for consistency.

Linear polarization measurements record the current response to a sweep of applied voltages, usually ranging from -30 mV to 30 mV in reference to the open circuit potential, which is determined by measuring the voltage of the test sample in reference to a reference electrode. As a reminder, the open circuit potential gives insight on a materials tendency to corrode in a specific environment. A material that increases in potential is said to shift anodically i.e. is less likely to corrode. While a decrease in the potential is said to shift cathodically i.e. more likely to corrode. The tendency of a metal to corrode can be easily confused with the corrosion rate, but it is very important to distinguish the two. While a material may have a high tendency to corrode, it can have a slow corrosion rate making it useful in specific applications. The corrosion resistance allows for the comparison of the corrosion rate for varying materials in a specific environment. The higher the corrosion resistance the slower the corrosion rate. The calculated slope from the linear polarization measurements equals the corrosion resistance. By comparing the open circuit potential

and the corrosion resistance the performance of the tested alloys can be evaluated.

The linear polarization measurements were made using a Parstat 4000 potentiostat. A Princeton Applied Research SCE was used as the reference electrode and a graphite rod was used as the counter electrode. The polarization voltage was swept from -30 mV to 30 mV in reference to the open circuit potential of the alloy sample at a rate of 1.667 mV/s. Once the linear polarization experiment was completed, the samples were rinsed with distilled water and rested for 24 hours before SEM images were taken with a Hitachi S-3000N.

In the series of experiments just discussed, the sample under test was submerged in the electrolyte while pulsed with current. This next series of experiments was performed to understand the impact from a salt fog. The impact of rep-rate pulse currents and high temperatures on the corrosion properties of 1018 steel, 8620 steel, 304 stainless steel, and 416 stainless steel was studied. The composition of these metals was shown earlier in Table 1. Once again, a novel test setup had to be developed so that so that a salt fog could be applied. The experimental setup used is shown in Figure 3-12. Because it was desirable to study the samples using surface characterization methods, their length had to be limited to 2". A custom salt fog chamber was fabricated using a polyvinyl chloride

(PVC) tee connector. The salt fog was passed through the two of the three ports while the third was used as a viewing port so that a Flir thermal imaging camera could make thermal measurements during the experiment. The third port was sealed using a thin piece of mylar and RTV silicon. In addition to the Flir thermal camera imaging, temperature measurements were made with a thermocouple attached to the rod sample outside of the salt-fog chamber.

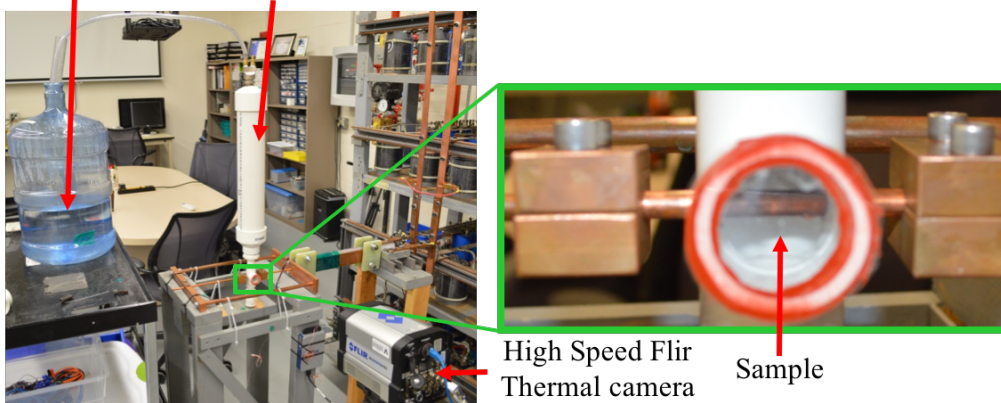Figure 3-12 Photographs of the pulsed current setup showing the connection of the sample and the placement within the salt fog chamber

The sample is attached to custom bus work and the same 63 kJ capacitive pulsed power supply is used to provide the pulsed current. Each rod has a diameter of 6.35 mm. A flat section was milled into the sample such that characterization using SEM and EDS could take place.

Because of the bottom of the sample is round, a small stand was created to hold the sample in the SEM, shown in Figure 3-13, holding it level.
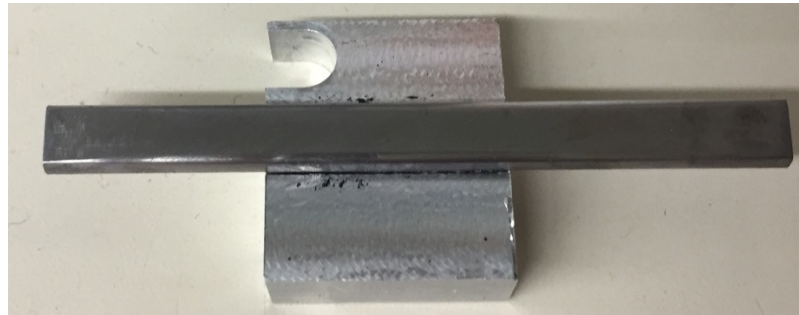
Figure 3-13 Sample being held on the sample stand

This series of experiments has three phases to it including an initial salt fog step, application of rep-rate pulse current, and a final salt fog. The initial salt fog exposure lasted one hour at a rate of 0.75 L/hr. An atomizing nozzle was used to create the salt fog from a bucket of salt water. After one hour of exposure, the sample was subjected to a series of current pulses while still within the salt fog. The initial current pulse was supplied with the power supply charged to 100 V while each of the nine subsequent pulses was supplied from the power supply charged to only 75 V. The higher initial charge was used to quickly raise the temperature of the sample and each subsequent pulse maintained the temperature without as steep of a temperature rise. Between each pulse, there was a rest period lasting one minute. Once the ten pulses were completed, the

sample was left in the salt for one additional hour. After the final one-hour salt-fog was completed, the sample was air dried for a minimum of twenty-four hours before being taken out. The sample was never rinsed off.

A second set of experiments that are identical to the pulsed experiments were performed with the only difference being that the samples were never pulsed with current. Instead the rods were exposed to the salt-fog only for a two hour 10-minute period.

A materials level characterization of each sample occurred before and after each experiment was performed. Each one was studied using SEM imaging and EDS to get a complete suite of information concerning its surface composition changes. Because characterization was performed before and after each experiment, comparisons could be made to understand the affect the salt-fog and pulsed current carry, respectively, had on the alloys' corrosion properties.

Figure 3-14 presents sample current measurements made when each of the four materials evaluated were pulsed with current with the power supply charged initially to 100 V. Figure 3-15 shows similar data for each respective material when the power supply was initially charged to 75 V. There is a 10% decrease in peak current between the two discharge voltages. The peak discharge current and FWHM pulse width measured during 100 V and 75 V pulsed discharges are presented in Table 4.
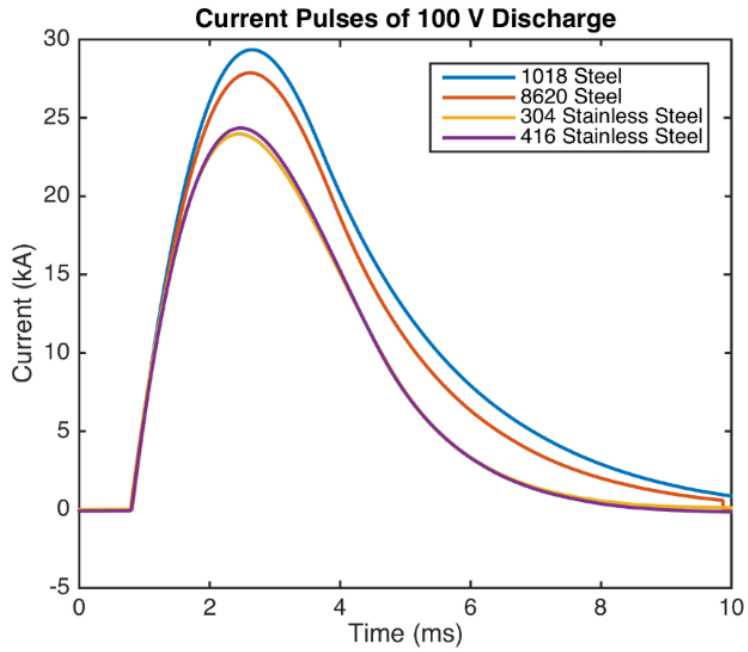
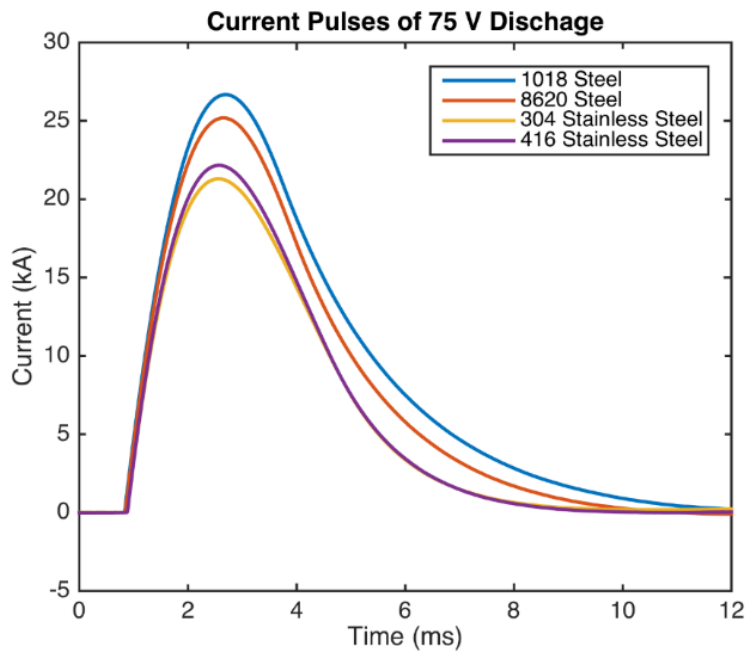Figure 3-14 Pulsed profile for 100 V discharge for all four alloys

Figure 3-15 Pulsed profile for 75 V dischage for all four alloys

64

The highest peak current and largest FWHM, respectively is measured
when a 1018 steel sample is used while the shortest of each is measured
when the 304 stainless steel sample is studied. This makes sense
because the 304 stainless steel has the highest overall resistivity.

Table 4 Peak current and pulsed widths measured from each respective sample when
pulsed using the 63 kJ pulsed power supply initially charged to 100 V and 75 V,
respectively

	100 V Discharge		75 V Discharge	
	Peak Current (A)	FWHM (ms)	Peak Current (A)	FWHM (ms)
304 Stainless Steel	24	3.1	21.3	3.1
416 Stainless Steel	24.4	3.1	22.2	3.1
1018 Steel	29.3	3.4	26.7	3.4
8620 Steel	27.9	3.2	25.2	3.2

Sample temperature profiles measured during a ten pulse
experiment with each sample are presented in Figure 3-16 through Figure
3-19. The 304 stainless steel sample reached the highest temperature of
154.7°C and had the highest average temperature of 79.6°C. The 1018
steel sample had the lowest peak temperature at 71.7°C with an average
temperature of 33.7°C.
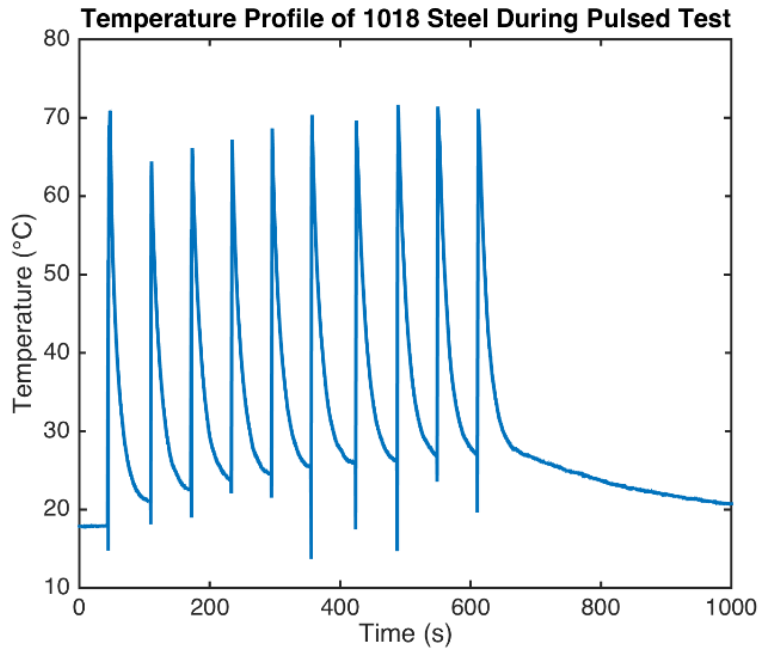
Figure 3-16 Temperature profile during the pulse test of 1018 steel
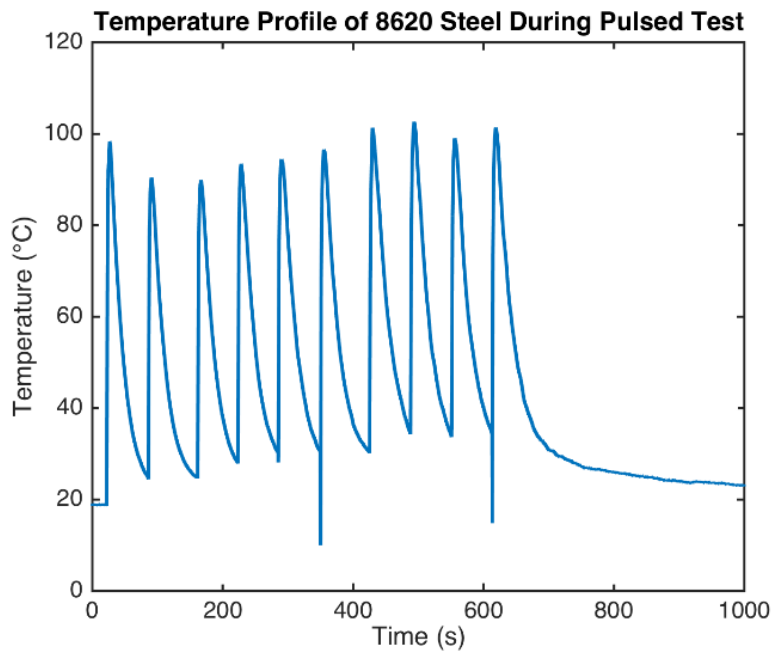
Figure 3-17 Temperature profile during the pulse test of 8620 steel
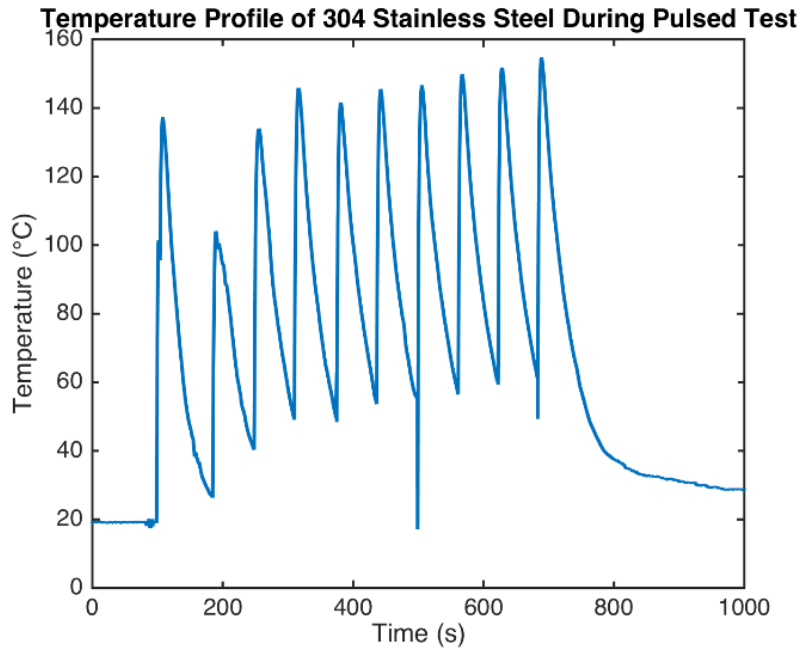
Figure 3-18 Temperature profile during the pulse test of 304 stainless steel
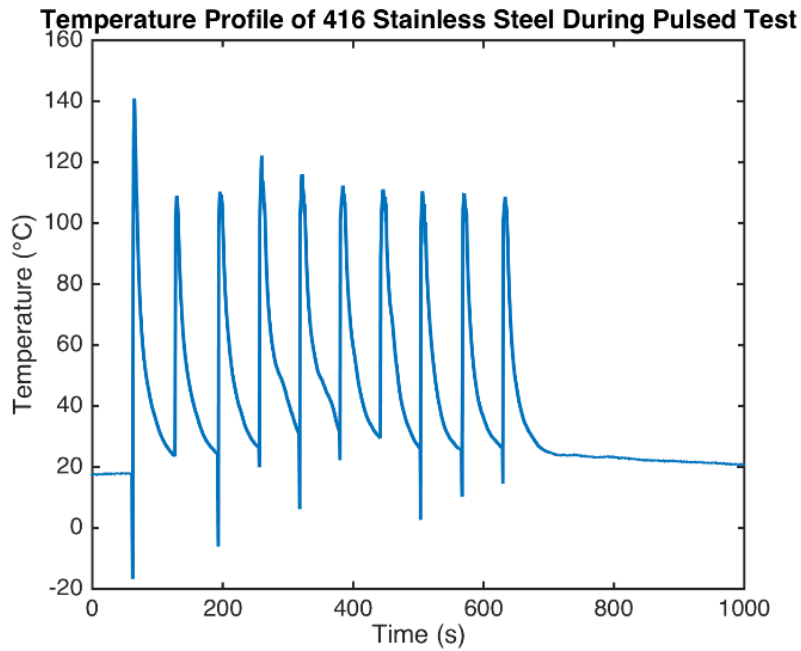
Figure 3-19 Temperature profile during the pulse test of 416 stainless steel

The 8620 steel sample reached a peak temperature of 102.6°C and averaged 53°C while the 416 stainless steel sample had a peak temperature of 141°C and an average temperature of 49.5°C. It is important to keep in mind that during each pulse, the stainless steel samples reached over 100°C, the 8620 steel sample reached over 100°C during only two of the ten pulses, and the 1018 steel sample never reached 100°C.

Chapter 4

Results and Discussion

Several experiments have been completed and will be reported on here that were aimed at better understanding the effect that magnetic fields have on the corrosion of metallic alloys. As previously mentioned, magnetic fields that were both externally applied as well as self-induced through high current flow were studied. The impact of an external DC magnetic field will be discussed first.

Corrosion Potential Measurements of Metallic Alloys in an Oxygen Saturated NaCl Solution with and without a Magnetic Field Present

Figure 4-1 and Figure 4-2 plot the impact a magnetic field has on the corrosion potential of 1018 and 8620 carbon steels respectively. Plots of the corrosion potential vs time are shown for two different experiments. The first is a baseline measurement when bare, untreated samples were used in an open-air NaCl solution and absent of a magnetic field. The second is from an experiment when bare samples were exposed to a DC magnetic field in an open-air NaCl solution. Note that only one measurement is shown for each metal sample in each test condition

69

however, the results are representative of what was measured from three

different experiments performed under identical conditions.
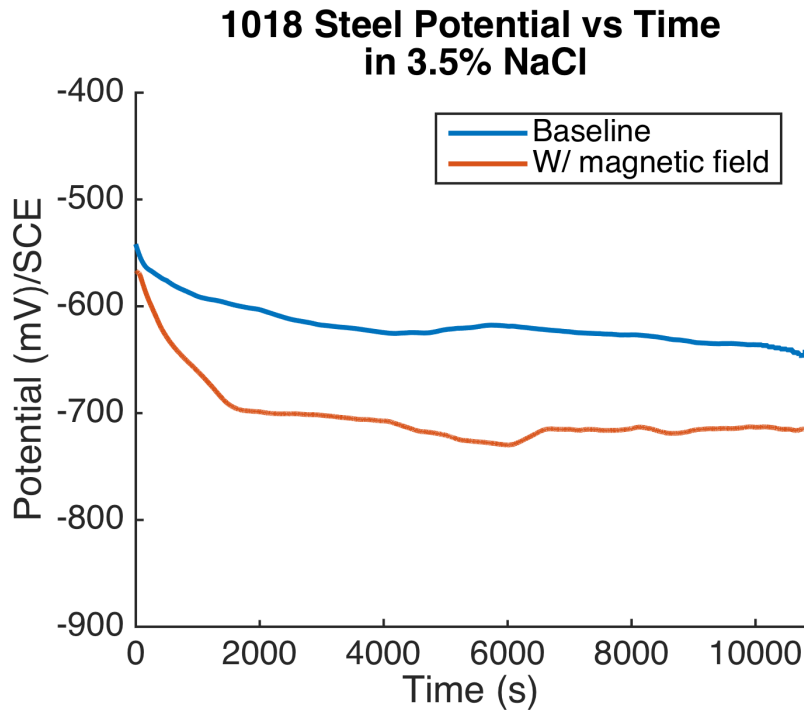
Figure 4-1 Corrosion potential of 1018 steel with and without a magnetic field present in

an air saturated electrolyte

Evaluation of each respective figure shows that the magnetic field

has a significant impact on the corrosion potential of both materials,

shifting them further in the cathodic, negative, direction. The corrosion

potential of 1018 steel shifted roughly 80 mV catholically on average when

the magnetic field was present while that of 8620 steel shifted roughly 73

mV catholically on average. This shift in potential is contributed to a

change in the oxygen concentration at the surface of the sample. The

magnetic field redistributes oxygen on the surface of the sample altering

the rate of reactions. As the oxygen concentration changes at the surface,

the cathodic reaction rate is altered affecting the corrosion potential when

the magnetic field is applied. A numerical analysis of this effect will be

discussed later. This cathodic shift in potential indicates that 1018 steel

and 8620 steel exposed to a magnetic field are less likely to corrode in a
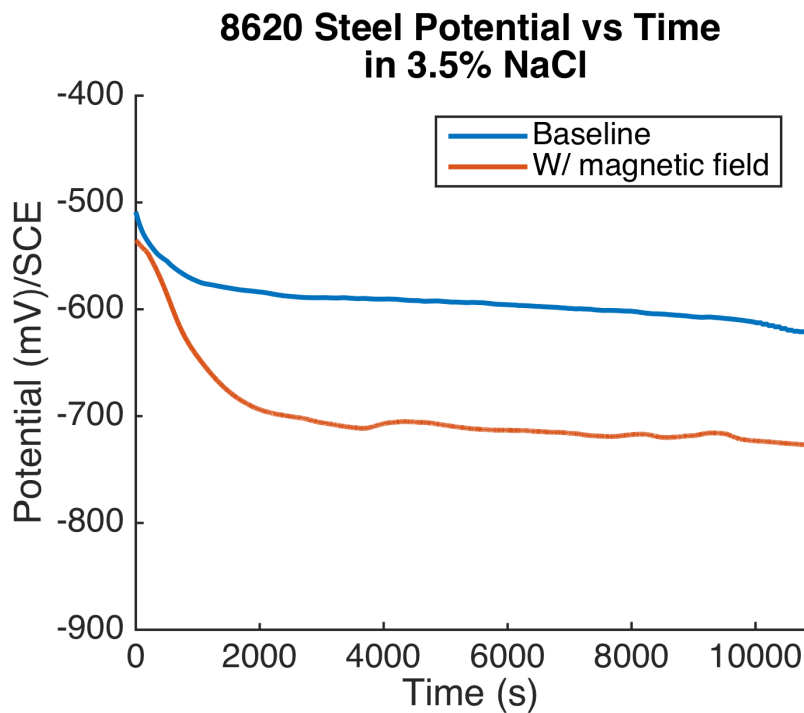
3.5% NaCl solution.

Figure 4-2 Corrosion potential of 8620 steel with and without a magnetic field present in

an air saturated electrolyte

When a magnetic field is present, the highly ferrous nature of these

metallic samples greatly enhances the magnetic field at edge of the

sample, as seen in Figure 3-4, which draws oxygen to the edges. The increased concentration of oxygen at the edge of the sample surface reduces the oxygen concentration at the center of the sample. This results in a total net decrease of oxygen concentration at the surface of the sample. This decrease in oxygen concentration will lower the potential of the cell. This hypothesis is backed up by the work documented by Ueno who found that under strong DC magnetic fields, dissolved oxygen would redistribute in the solution [27]. These results illustrate how a magnetic field can impact the reaction rates of corrosion for metallic alloys.

Figure 4-3 and Figure 4-4 plot the corrosion potential vs. time measurements made when each of the two respective stainless steel alloys were tested. Results are presented for identical conditions as presented for 1018 and 8620 steels earlier. When viewing the corrosion potential measurements of nonmagnetic 304 stainless steel, seen in Figure 4-3, it should be noticed that the magnetic field has an almost negligible impact on the corrosion potential. If anything, the corrosion potential shifted more anodic, with a potential change of roughly 12 mV on average in the negative direction, when the magnetic field was present. The small shift in potential signifies that 304 stainless steel when exposed will have the same tendency to corrode as without a magnetic field in 3.5% NaCl. It is believed that the minimal impact is a result of the

nonmagnetic nature of 304 stainless steel. While the magnetic field does

have an impact on both the free ions and the oxygen in the electrolyte, the

non-magnetic nature of 304 stainless steel does not heavily alter the

oxygen concentration on the surface so there is a minimal impact to the

rate of corrosion reactions.

304 Stainless Steel Potential vs Time in 3.5% NaCl

Figure 4-3 Corrosion potential of 304 stainless steel with and without a magnetic field present in an air saturated electrolyte

Figure 4-4 plots the corrosion potentials measured from mildly

magnetic 416 stainless steel metal under conditions identical those

evaluated for the three earlier materials. The results show that the

magnetic field has a very small impact on the corrosion potential, shifting it

more anodic, with a shift of 21 mV in the positive direction on average.

This anodic shift indicates that that even a weakly magnetic material will

impact the magnetic flux enough to draw more oxygen to the surface, but

not as heavily redistribute the oxygen concentration on the surface of the

sample. The higher anodic potential indicates that 416 stainless steel will

have a lower tendency to corroded when exposed to an external magnetic

field in 3.5% NaCl.

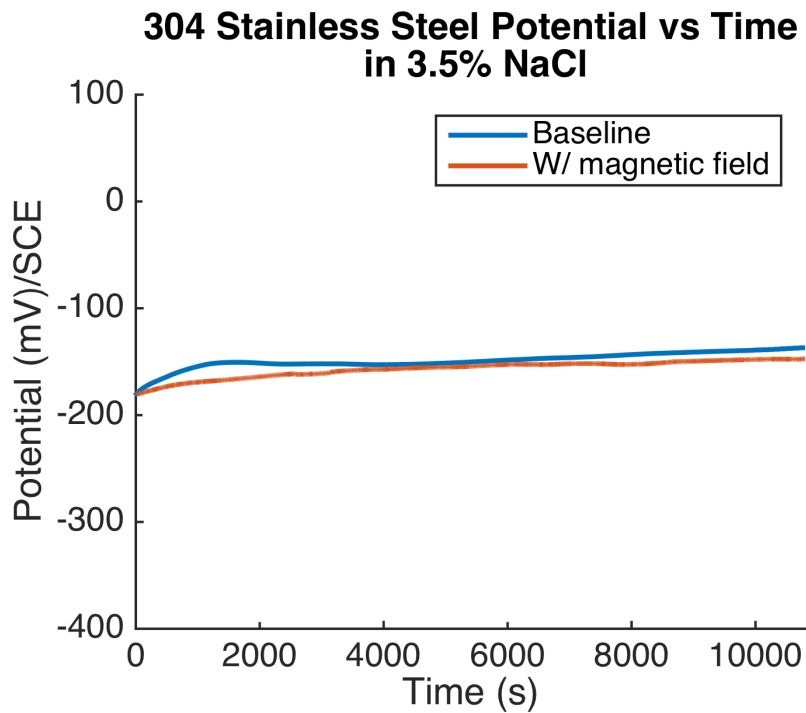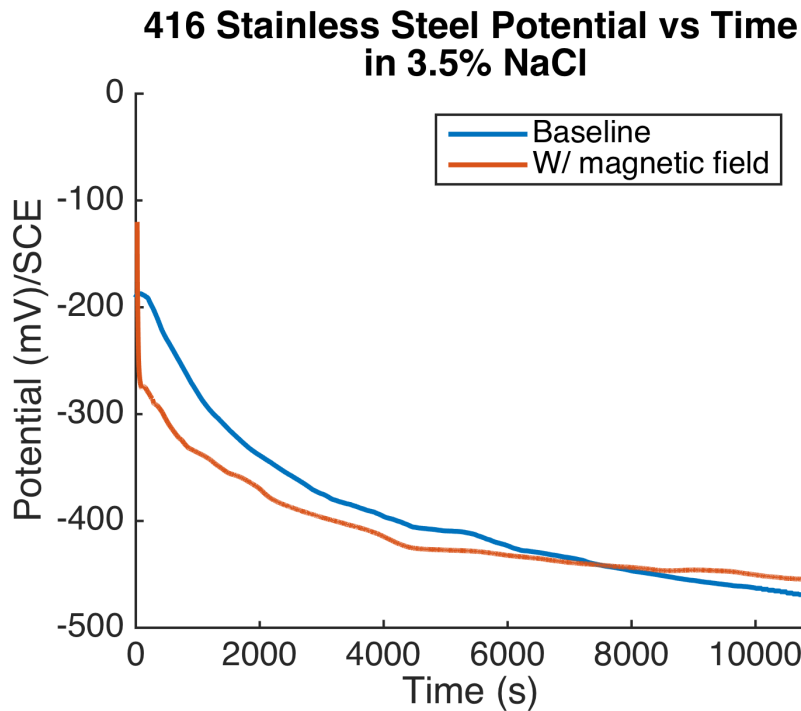Figure 4-4 Corrosion potential of 416 stainless steel with and without a magnetic field
present in an air saturated electrolyte

Figure 4-5 shows macro and scanning electron microscope (SEM)

scale images taken of the four respective bare samples evaluated both

with and without exposure to a magnetic field. The SEM images provide a better understanding of how the magnetic field influences the location of the anodic reactions. The SEM images taken of the 1018 steel, the 8620 steel, and the 416 stainless steel samples respectively, show a lower pitting density at the center of each sample than is present along their outer edges. The pitting density along the edges is similar to that observed nearly uniformly on the baseline sample's surface. When a magnetic field is applied, oxidation growth is seen in a ring around the center of the sample on the 1018 and 8620 steel samples. On the samples that were not exposed to a magnetic field, pitting is seen throughout the samples surface. This is an indication of the magnetic field affecting the oxygen concentration at the surface of the alloy. When the magnetic field is applied, the magnitude of the magnetic field is largest at the edges of the highly ferromagnetic alloys. The higher strength magnetic field attracts the paramagnetic oxygen to the edges increasing the oxidation formation in these regions. This shows how the magnetic field most heavily impacts the location where pitting occurs and that given prolonged exposure to a magnetic field, as will occur on future naval vessels, the magnetic field will greatly influence how metals corrode.
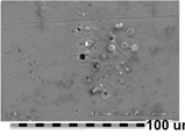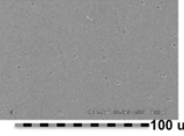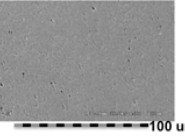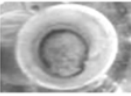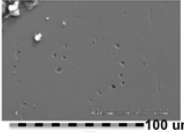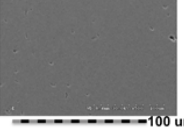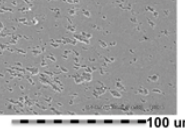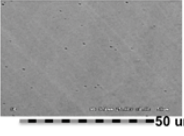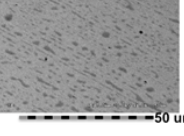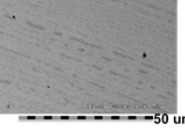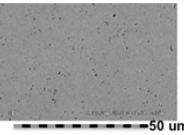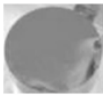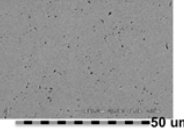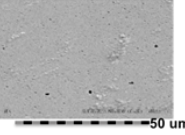
Figure 4-5 SEM and photographic images of the bare 1018 steel, 8620 steel, 304 stainless steel, and 416 stainless steel samples respectively.

While the macro scale images taken of the two respective 304 stainless steel samples appear to show negligible differences between the two, the SEM images show that the sample exposed to a magnetic field has a lower density of pitting than the baseline sample does. This is expected because the there is no magnetic field gradient along the surface of the alloy. Thus, the pitting is uniform like that of the baseline sample.

Numerical Analysis on the Open Circuit Potential of 1018 Steel Using the Nernst Equation

The Nernst equation relates the potential of a half-cell to the temperature, pressure, standard electrode potential, and reactions of the materials used. For simplicity, we will assume 1018 steel is 100% iron. To determine the reaction that will occur the Pourbaix diagram of iron is used, shown in Figure 4-6.

As seen in the figure, the resulting product is dependent on the pH of the solution and the half-cell potential of the reduction reaction. The potential in the diagram is in reference to the standard hydrogen electrode (SHE). For the baseline sample of 1018 steel in 3.5% NaCl solution the open circuit potential was –630 mV vs. the saturated calomel electrode (SCE). After converting to the SHE the potential would be –386 mV. Since

the pH is 7 and the potential is -386 mV, the resulting product would be Fe^{2+}.
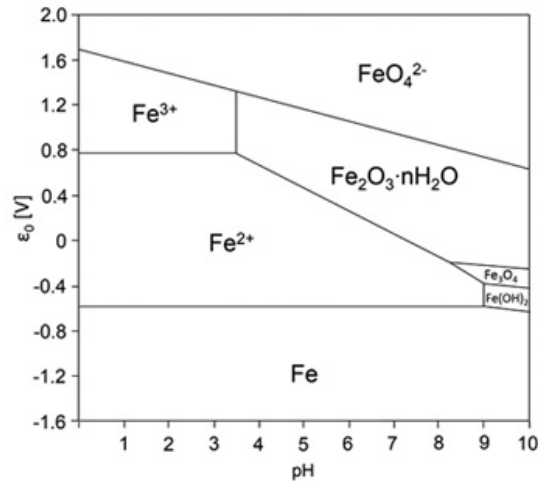
Figure 4-6 Iron Pourbaix diagram [34]

A few cathodic reactions will occur in a water solution. The cathodic reaction that will occur is based off the pH level of the solution. The cathodic reaction for NaCl with a weight percent of 3.5% in water is:

$$O_2 + 4H^+ + 4e^- \rightarrow 2H_2O \tag{2}$$
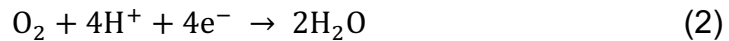
The Nernst equation is defined as:

$$E_{red} = E_{red}^0 + 2.3026 * \frac{RT}{zF} \log \frac{a_{Ox}}{a_{Red}} \tag{3}$$

E_{red} is the half-cell reduction potential. E^0_{red} is the standard half-cell reduction potential. R is the universal gas constant. T is the temperature in kelvin. Z is the number of moles of electrons transferred. F is the Faraday constant and a_{ox} and a_{red} is the chemical activity or the oxidizing agent and the reducing agent, respectively.

Taking, the cathodic reaction shown above and assuming there a limitless supply of solution at room temperature, the Nernst equation for the reduction reaction will become:

$$E = 1.23 - 0.059\text{pH} + 0.01475 \log \frac{1}{P_{O_2}} \qquad (4)$$

As seen in the equation, the potential is a function of pH and the partial pressure of oxygen, which is related to the concentration of oxygen at the surface. A higher pressure would indicate a higher oxygen concentration. As mentioned before the NaCl solution used would have a pH of 7, therefore the reduction potential would be:

$$E = 0.817 + 0.01475 \log \frac{1}{P_{O_2}} \qquad (5)$$

The equation for the potential of the entire cell is calculated from the half-cell oxidation and reduction potentials:

$$E_{cell} = E_{ox} - E_{red} \qquad (6)$$

By assuming the pressure of oxygen is at atmosphere E_{cell} can be calculated.

$$E_{cell} = -0.3856 + 0.817 + 0.01475 \log 0.21 = 0.4084 \text{ V} \qquad (7)$$

The cell potential is required to stay constant in order for the system to stay in equilibrium. By rearranging the equation, E_{ox} can be seen as a function of oxygen pressure.

$$E_{ox} = -0.3366 - 0.01475 \log \frac{1}{P_{O_2}} \qquad (8)$$

The oxidation potential as a function of oxygen is shown in Figure 4-7. As oxygen concentration decreases so does the oxidation potential. This would correlate with the results shown before. The magnetic field strength being highest at the edges of the sample would result in a higher oxygen concentration at the edges.
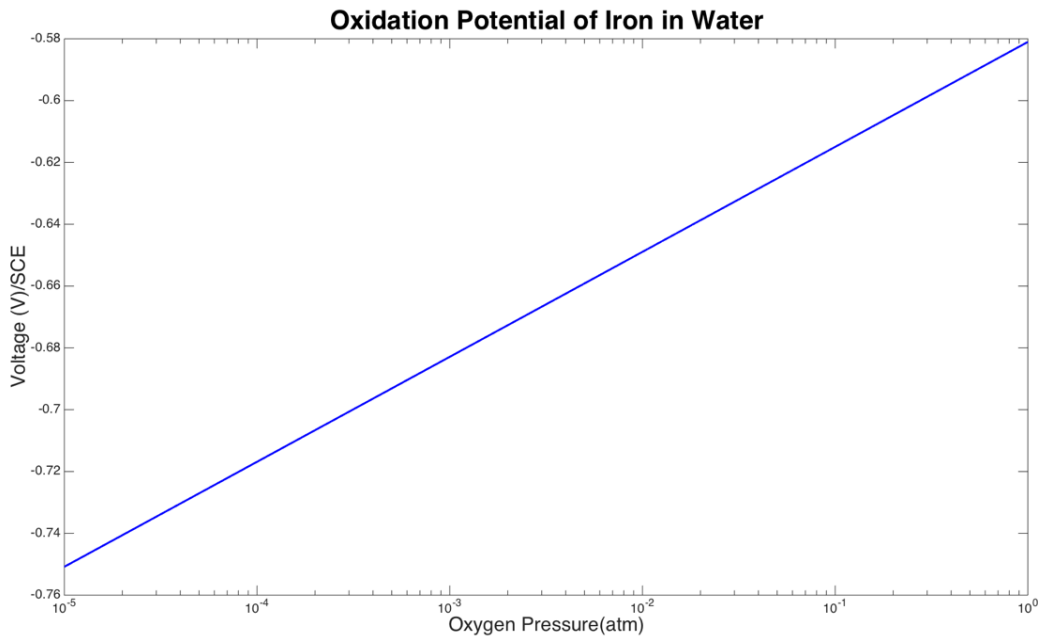
Figure 4-7 Oxidation potential of iron as a function of oxygen pressure

Increasing the concentration at the outer edges would decrease the oxygen concentration at the center of the sample resulting in a net decrease of oxygen across the surface of the sample and a reduction in the oxidation potential. This effect is the reason for the decrease in potential with the magnetic field applied in the experiments shown above. If oxygen concentration was to increase at the

surface, such as the case with 416 stainless steel, the potential will increase as seen in the open circuit and anodic polarization measurements.

Corrosion Potential Measurements in Air and Argon Saturated Electrolytes with and without a Magnetic Field Present

In an effort to confirm that the paramagnetic nature of oxygen is what dominates the change in the corrosion potential of the alloys presented earlier, several experiments were performed with argon to displace dissolved oxygen in the electrolyte. Shown below in Figure 4-8 through Figure 4-11 are corrosion potential measurements made in both air and argon saturated electrolytes respectively for each of the four respective metals presented earlier. During each experiment, the sample is exposed to a magnetic field and there is time when they are not exposed to a magnetic field. The materials were allowed to rest for three hours without a magnetic field applied to allow for the potentials to stabilize at the open air corrosion potential. After three hours had passed, the magnetic field was turned on without any other alteration to the test cell, which was done to determine if the corrosion potential would change depending on if the solution was air or argon saturated. As seen below, when the electrolyte is saturated with air, there is an almost immediate shift in the potential in the cathodic direction when the magnet is turned on for the 1018 steel and 8620 steel samples. This indicates a higher tendency to corrode in the air saturated solution with the magnetic field turned on. It is also important to realize that the magnetic field can impact the corrosion mechanisms almost immediately, which

indicates time varying magnetic fields would also have an impact on corrosion properties. The immediate change in potential indicates that the oxygen concentration at the surface is changing almost instantaneously. The corrosion potentials of 1018 steel, 8620 steel, and 416 stainless steel show the most dramatic shift with the degree of shift heavily dependent again on the material's permeability. In the case of 304 stainless steel, there is no observed shift in the potential when the magnetic field is applied in either the oxygen or argon saturated electrolyte.

It is important to notice that when the electrolyte is saturated with argon, there is an almost negligible impact on the corrosion potential in any of the materials when the magnetic field is applied. Since there is no paramagnetic oxygen in the electrolyte, the magnetic field does not redistribute oxygen at the metal surface and therefore there is no measured change in the corrosion potential. The potentials of 1018 steel, 8620 steel, and 416 stainless steel in the argon saturated electrolyte have a lower potential than those measured when the electrolyte was saturated with air. This correlates with the results shown in the numerical analysis of 1018 steel. The same reason the potential decreases with argon present is the same reason the potential decreases when the external magnetic field is applied as the oxygen concentration on the surface of the sample has decreased. The potentials measured in the argon saturated solution is close to the absolute minimum the potential of a sample in an air saturated would be able to reach when subjected to a magnetic field.

1018 Steel Potential vs Time in 3.5% NaCl
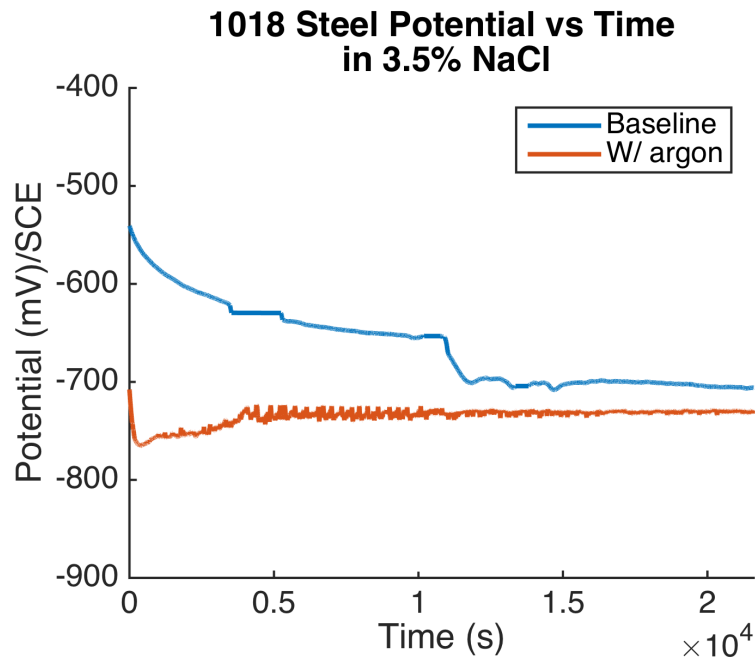
Figure 4-8 Corrosion potential of 1018 steel in both air saturated and argon saturated

electrolytes respectively

8620 Steel Potential vs Time in 3.5% NaCl
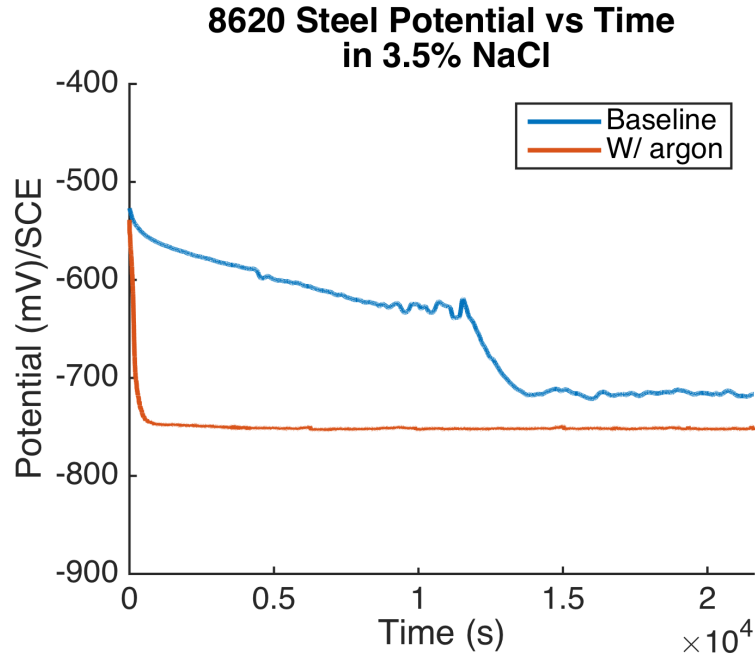
Figure 4-9 Corrosion potential of 8620 steel in both air saturated and argon saturated

electrolytes respectively
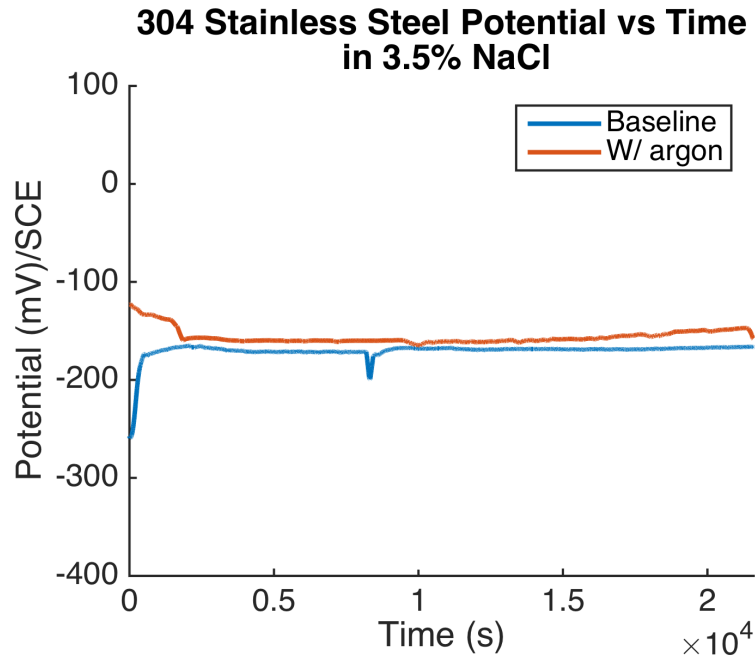
Figure 4-10 Corrosion potential of 304 stainless steel in both air saturated and argon saturated

electrolytes respectively
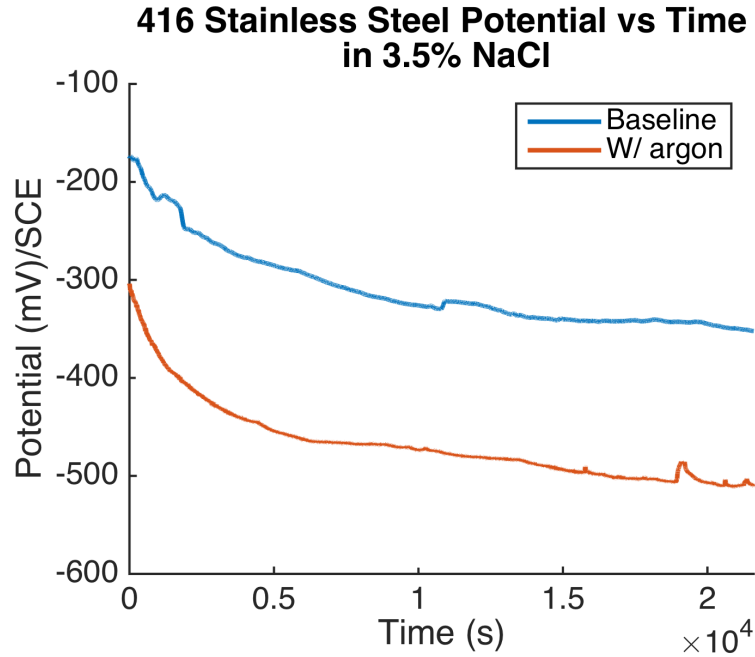
Figure 4-11 Corrosion potential of 416 stainless steel in both air saturated and argon saturated

electrolytes respectively

Anodic Polarization Measurements with and without an Externally Applied DC Magnetic Field

In the next set of experiments, the three-electrode setup was used to perform the anodic polarization technique. After the samples were submerged in the solution for three hours, the anodic polarization measurement was started. The samples evaluated include: 304 stainless steel, 416 stainless steel, 1018 steel, 8620 steel, C110 copper, C182 copper, 6061-T6 aluminum, and 7075-T6 aluminum. The copper and aluminum samples were added to evaluate additional alloys with different compositions. Figure 4-12 through Figure 4-19 show the results of the anodic polarizations measured for each respective alloy. Figure 4-12 shows the anodic polarization results for 304 stainless steel.
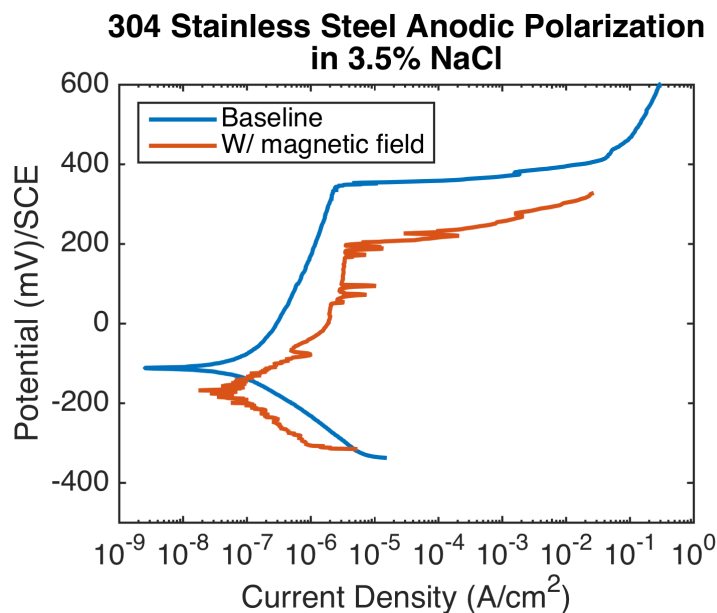
Figure 4-12 Anodic polarization of 304 stainless steel in 3.5% NaCl solution

The first observation is the cathodic shift in corrosion potential when the external magnetic field is applied, which was seen in the corrosion potential results shown earlier. 304 stainless steel is an active-passive metal. The transpassive potential of the baseline sample begins at 0.38V. This is the potential at which the metal begins to pit. There is a shift in both potentials when the sample was subjected to a magnetic field. The transpassive potential decreased by 0.18V indicating that it is easier for the sample exposed to the magnetic field to oxidize in specific solutions, but it will begin to pit before the baseline sample will. The other important change is the increase in passivation current when the sample was exposed to a magnetic field. The sample exposed to the magnetic field has a higher corrosion rate in the passivation region than the baseline sample does in the passivation region. In comparison, the sample exposed to a magnetic field will be subjected to a higher corrosion rate than the baseline sample in the same solution.

The plot of the anodic polarization of 416 stainless steel is shown in Figure 4-13. Unlike the 304 stainless steel sample there is no well-defined passivation region. 416 stainless steel will still passivate, but the region in which it can is small. The sample that was subjected to the magnetic field has an increase in the corrosion potential, which is opposite to what was seen in the open circuit potential measurements. This could be contributed to the active changing of the potential, which could alter the corrosion potential. Since, the change in open circuit potential was already small, any active changes of the

cell could alter the potential enough to change the potential in the opposite way. There was an increase in the corrosion current density when the sample was subjected to the magnetic field. The increase in corrosion current density indicates an increase in charge transfer at the equilibrium state of 416 stainless steel. Similar to the 304 stainless steel sample the sample subjected to the magnetic field will experience higher corrosion rates in similar environments.

416 Stainless Steel Anodic Polarization in 3.5% NaCl
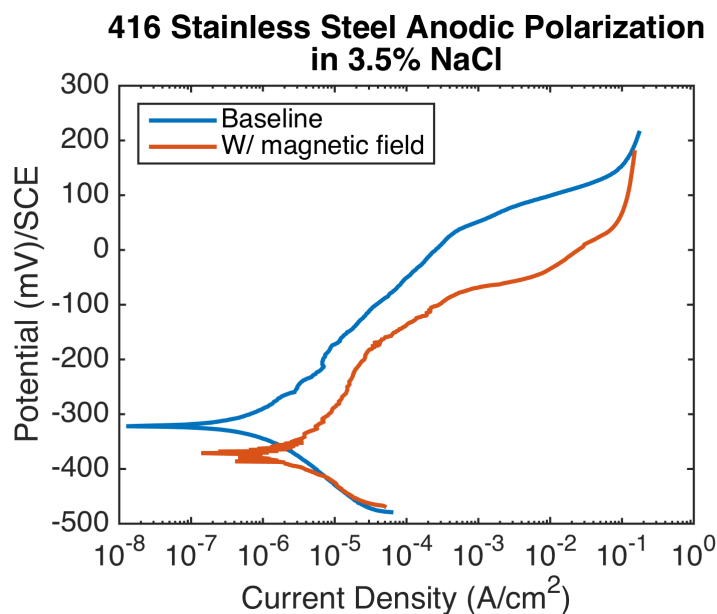
Figure 4-13 Anodic polarization of 416 stainless steel in 3.5% NaCl solution

Figure 4-14 plots the anodic polarization curve of 1018 steel in a 3.5% NaCl solution. As seen in the plot there is no passivation region observed for 1018 steel. 1018 steel is a low carbon steel, which is the most common steel used. Unlike the stainless steel samples, which is made with chromium to form a passive layer, 1018 steel has zero chromium content. Since 1018 steel is an active metal there is no passivation region observed in the plot. An active metal

does not have a passivation region and will corrode at all potentials within this type of environment. The potential of the metal decreased in the cathodic direction when the external magnetic field was applied. The corrosion current density decreased when the sample was subjected to the magnetic field. From the change in current density measured, it can be inferred that this sample will have a lower corrosion rate than the baseline sample in a 3.5% NaCl solution will. Another point of interest is the increased slope in the active region as the potential increases between the sample exposed to the magnetic field and the baseline sample. This means that in some cathodic reactions, the intersection is at a higher point and the 1018 steel sample subjected to the magnetic field will have a lower corrosion rate.
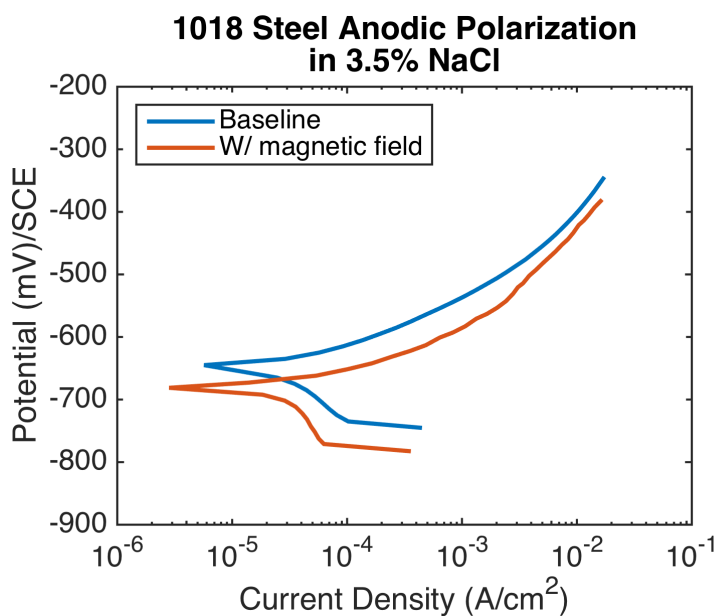
Figure 4-14 Anodic polarization of 1018 steel in 3.5% NaCl solution

The anodic polarization plot for 8620 steel in 3.5% NaCl solution is shown in Figure 4-15. 8620 steel has higher chromium content than 1018 steel, but not enough to classify it as a stainless steel. Similar to 1018 steel, the corrosion potential decreased with exposure to an externally applied DC magnetic field. The slope in the active region of the sample subjected to the magnetic field increased faster than the baseline sample, which is a similar trend to the 416 stainless steel and 1018 steel experiments seen earlier. At the higher potentials, the current density is similar between the baseline and magnetic field sample. At lower potentials 8620 steel will corrode slower when exposed to a magnetic field, but at the higher potential 8620 steel would behave like the baseline.

8620 Steel Anodic Polarization in 3.5% NaCl
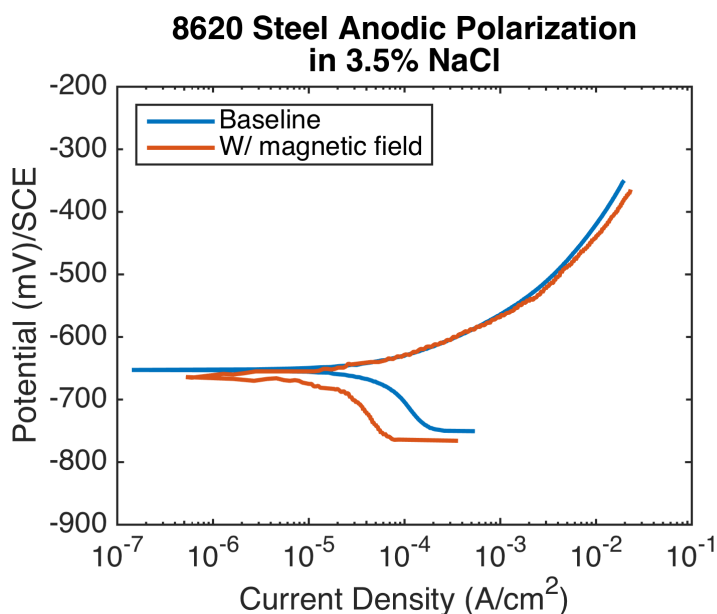
Figure 4-15 Anodic polarization of 8620 steel in 3.5% NaCl solution

The copper and aluminum alloys were added in the anodic polarization tests to determine the impact of magnetic fields on different alloys other than those that are iron based. These alloys were selected because of their highly conductive properties. Evaluating diamagnetic materials with high conductivity provides a broader understanding of the impact magnetic fields has on the corrosion of alloys.

The C110 copper anodic polarization curves are shown in Figure 4-16 and those of C182 are shown in Figure 4-17. Both plots show a small region of passivation and the passivation potential is the same for both samples at roughly -0.05 V vs. SCE.
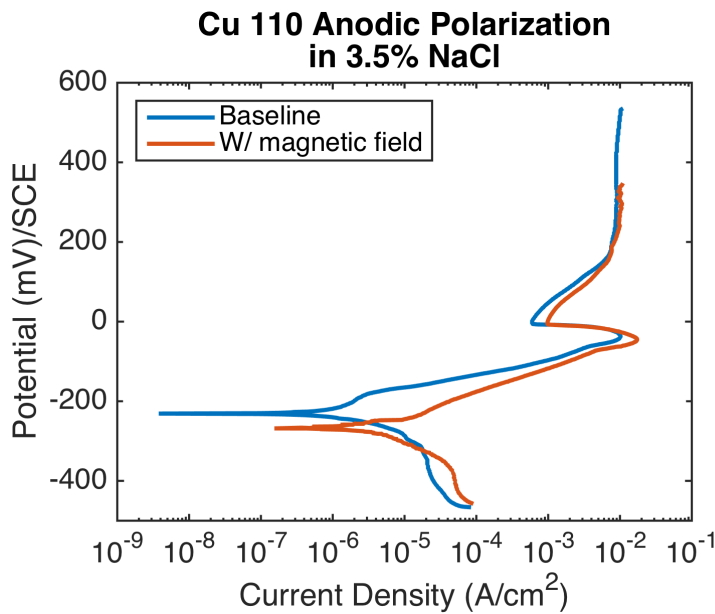
Figure 4-16 Anodic polarization of copper 110 in 3.5% NaCl solution

The passivation current density for the C110 sample subjected to a magnetic field is higher than the baseline sample while the critical current

density is higher on the sample subjected to the magnetic field. The corrosion

potential of the C110 sample shifted cathodically when it was exposed to a

magnetic field as compared to the baseline sample. The corrosion current

density was also higher on the sample subjected to the magnetic field. The

changes between the sample exposed to the magnetic field and the baseline

sample are diminished in this material, similar to the differences observed in

304 stainless steel as expected since both materials are diamagnetic. These

changes indicate that the amount of change in the cathodic reaction is related

to the strength of the magnetic field near the sample.
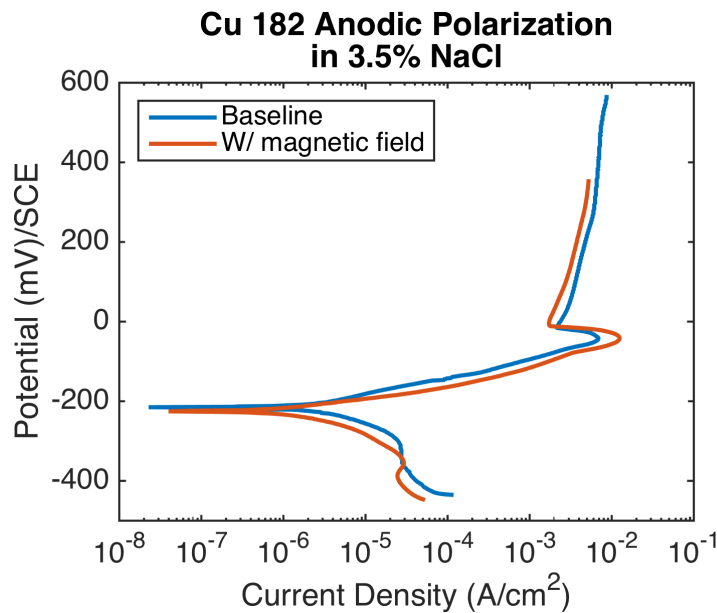
Figure 4-17 Anodic polarization of copper 182 in 3.5% NaCl solution

In Figure 4-17, there is a small shift in the potential between the C182

sample exposed to the magnetic field and the baseline sample. The change in

corrosion potential between the two samples is less than 10 mV and they can

likely be attributed to small change in the setup. It appears that C182 sees the least amount of effect from exposure to the magnetic field.

Figure 4-18 shows the anodic polarization curves of Al 6061 in 3.5% NaCl solution. There is a small shift in the corrosion potential in the cathodic direction when the sample was subjected to the magnetic field. The corrosion current density decreased when exposed to the magnetic field in comparison to the baseline sample. The current density rapidly increases in the presence of a magnetic field compared to the baseline sample. This indicates that at higher potentials Al 6061 will corrode faster when exposed to the magnetic field compared to the baseline sample.
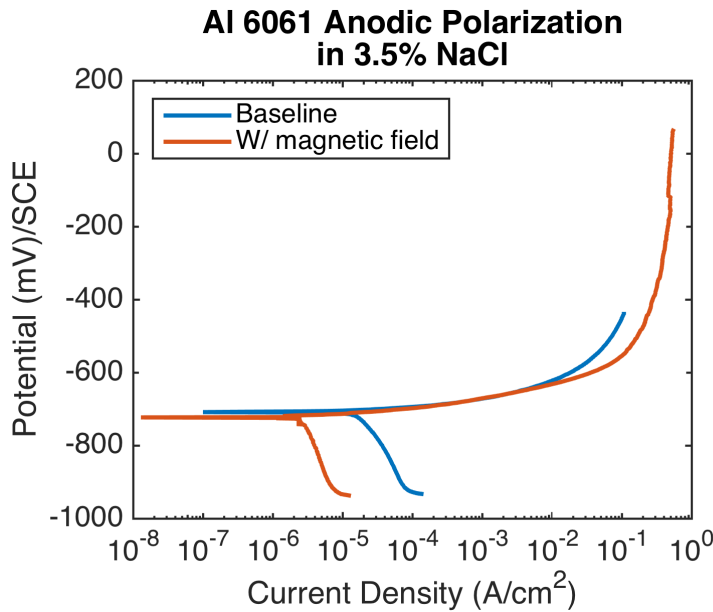
Figure 4-18 Anodic polarization of aluminum 6061 in 3.5% NaCl solution

The anodic polarization curves of Al 7075 in 3.5% NaCl is shown in Figure 4-19. This metal experienced a dramatic change with the exposure to

the magnetic field. The potential shifted anodically with the exposed magnetic

field and removed the passivation region seen in the baseline sample. The

corrosion current density also increased when the sample was exposed to the

magnetic field. At the higher anodic potentials, the current density was an order

of magnitude less than measured from the baseline counterpart. These shifts

indicate that when Al 7075 is subjected to a magnetic field the alloy will not

passivate and will corrode faster at higher potentials in 3.5% NaCl.

Al 7075 Anodic Polarization in 3.5% NaCl
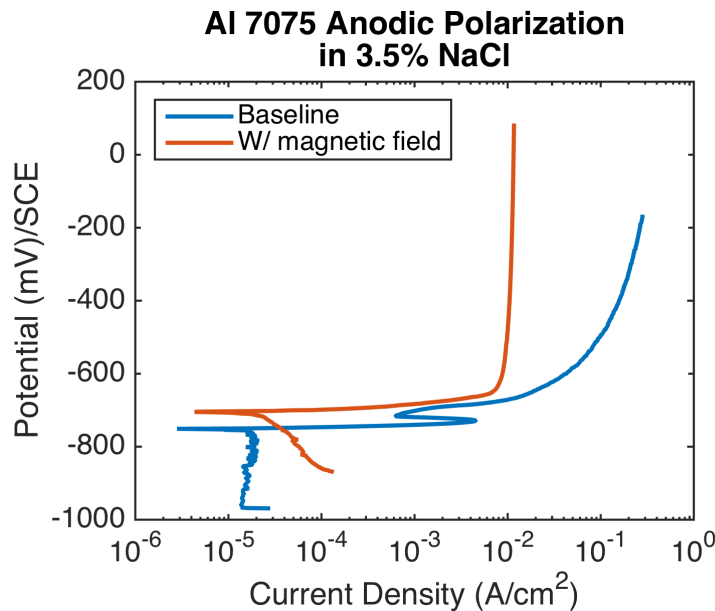
Figure 4-19 Anodic polarization of aluminum 7075 in 3.5% NaCl solution

Linear Polarization Measurements with and without High Pulsed Current Carry

The next set of experiments to be discussed here are those in which

6.35 mm rod samples were pulsed with between 6 kA and 9 kA current,

depending upon material, while submersed in 800 ml of 3.5% NaCl solution.

Each rod sample was pulsed with current every ten minutes over a three-hour period, totaling nineteen times. After each three-hour test series was completed, linear polarization measurements were made. The linear polarization results obtained from the 1018 steel and 8620 samples respectively are shown in Figure 4-20 and Figure 4-21. As shown earlier in Figure 3-9, each of these samples was pulsed with roughly 9 kA of current during each pulse.

In the case of 1018 steel, the linear polarization results show that both the corrosion potential and the corrosion resistance decreased after exposure to the pulsed current and induced magnetic field. This is evident from several factors that should be noted in the Figure 4-20.

Figure 4-20 Linear polarization measurements of 1018 steel with and without pulsed current in 3.5% NaCl in open air at room temperature

First, there is a slight change in the slope of the polarization curves, orange being the slope of the baseline sample and aqua being the slope of the

pulsed sample. A decreased slope means that the corrosion resistance is decreased and therefore that the corrosion rate is increased when the rods are subjected to a pulsed current. Second, the corrosion potential is shifted downward indicating that the alloy is slightly less active. In the case of 8620 steel, shown in Figure 4-21, the corrosion potential decreased but the corrosion resistance increased after exposure to the pulsed current and magnetic fields.
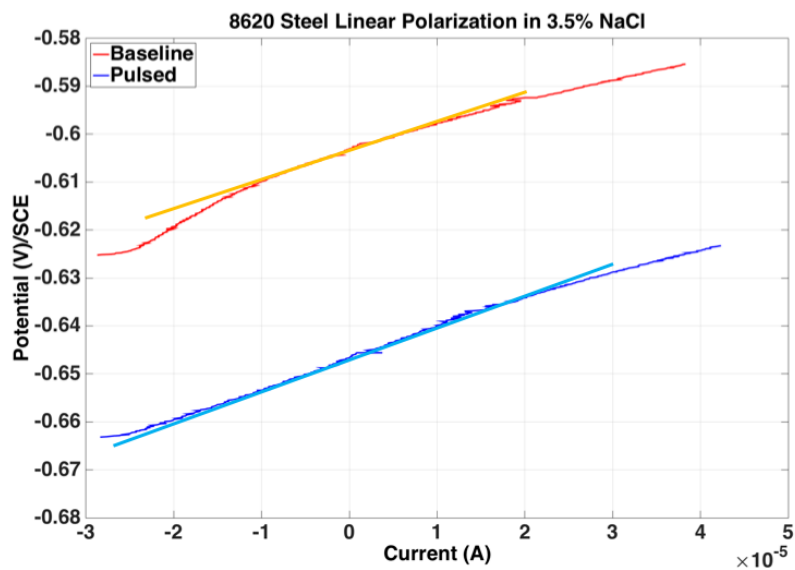
Figure 4-21 Linear polarization measurements of 8620 steel with and without pulsed current in 3.5% NaCl in open air at room temperature

As mentioned before, this is evident from the change in slope between the baseline and pulsed samples, respectively. As seen in the Figure 4-21, the slope increased after exposure to magnetic fields corresponding to an increase to the corrosion resistance. The increased corrosion resistance is equivalent to a decrease in the corrosion rate. The corrosion potential decreased similar to

the way 1018 steel did indicating that 8620 is less active after being exposed to the pulsed magnetic fields.

Figure 4-22 presents the linear polarization measurements from the 304 stainless steel and 416 stainless steel samples, respectively. It is important to note that the 304 stainless steel is austenitic, i.e. non-magnetic, while 416 stainless steel, 1018 steel, and 8620 steel all have permeability greater than 1.
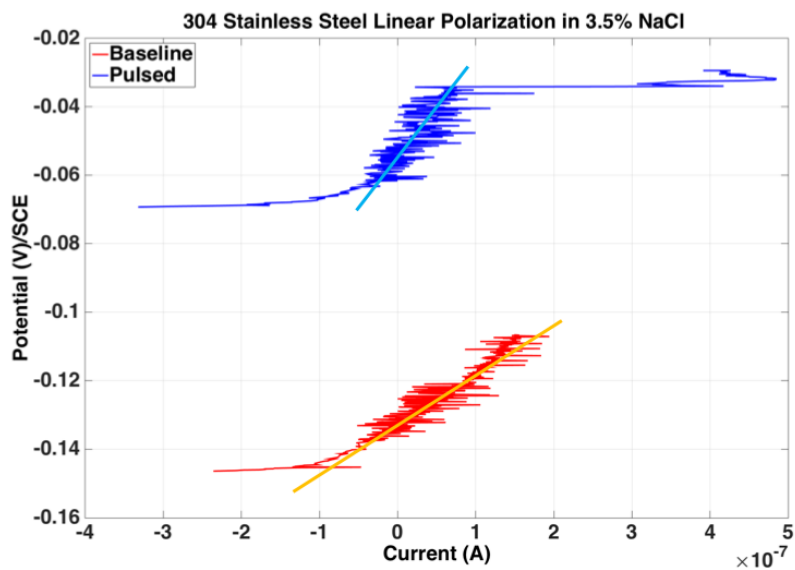
Figure 4-22 Linear polarization measurements of 304 stainless steel with and without pulsed current in 3.5% NaCl in open air at room temperature

As shown earlier, the ferromagnetic properties of the material impact the magnetic field gradient and magnetic flux density across the samples surface. 304 stainless steel's lack of permeability alters the direction the corrosion potential shifts when compared with how it shifts for each of the other three materials.

In the case of 304 stainless steel, shown in Figure 4-22, the corrosion

potential increases indicating that it has become a more less active alloy after

exposure to pulsed current and their induced magnetic fields. This means there

is a decrease in the material's corrosion tendency decreasing its likelihood of

corroding. In addition to the increase in corrosion potential, the corrosion

resistance of 304 stainless steel increased with the exposure to pulsed

currents. The corrosion potential of 416 stainless steel, shown in Figure 4-23,
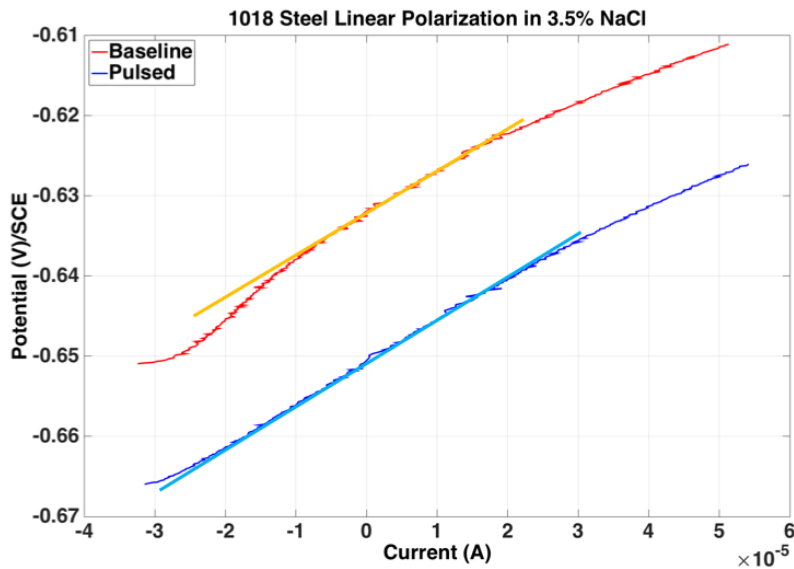
decreased meaning that this alloy becomes more active.
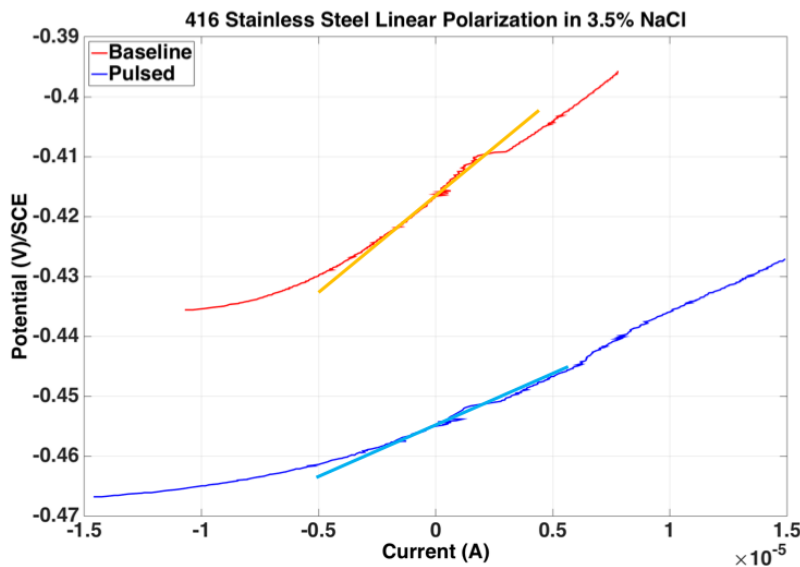
Figure 4-23 Linear polarization measurements of 416 stainless steel with and without pulsed

current in 3.5% NaCl in open air at room temperature

All of the changes from each of the four materials evaluated are

summarized in Table 5. 416 stainless steel has the same trends as the 1018

steel sample while the 304 stainless steel sample was impacted differently than

all of the other alloys. The variation in corrosion potential and corrosion

resistance observed between each of the respective baseline and pulsed

samples is believed to be a result of the oxygen that is dissolved in the

electrolyte being influenced by the magnetic field.

Table 5 Linear polarization measurements extrapolated from the linear polarization experiments

of the pulsed and baseline samples

Material	Experiment	Corrosion Potential (mV)	Corrosion Resistance (Ω)	What it Means
1018	Baseline	-632.4	582.0	1018 steel will corrode faster and has a higher tendency to corrode when subjected to a pulsed current
	Pulsed	-650.7	536.1	
8620	Baseline	-603.4	606.2	8620 Steel will corrode slower and has a higher tendency to corrode when subjected to a pulsed current
	Pulsed	-648.8	671.0	
304	Baseline	-132.1	152.0 k	304 stainless steel will corrode slower but has a lower tendency to corrode when subjected to a pulsed current
	Pulsed	-54.2	277.4 k	
416	Baseline	-416.8	2.9 k	416 stainless steel will corrode faster but has a higher tendency to corroded when subjected to a pulsed current
	Pulsed	-459.2	1.8 k	

As in the previous experiments, it is believed that oxygen's paramagnetic

nature allows it to be moved by the magnetic fields, altering its concentration

near the electrode surface. That change in concentration alters the kinetics of

the system and changes the corrosion potential and corrosion resistance,

respectively. The variation in the corrosion potential shift between ferromagnetic

and diamagnetic materials suggests that permeability of the alloy significantly

influences the rate of corrosion and thus the resistance. Though experiments

with argon may have helped to better prove the impact of oxygen, these types

of experiments were not performed.

After each linear polarization measurement was made, SEM images were taken of each sample for visual examination of the changes to the corrosion and pitting of the surface. Figure 4-24 presents the images taken after the baseline and pulsed experiments evaluating 1018 steel and 8620 steel respectively, were completed.
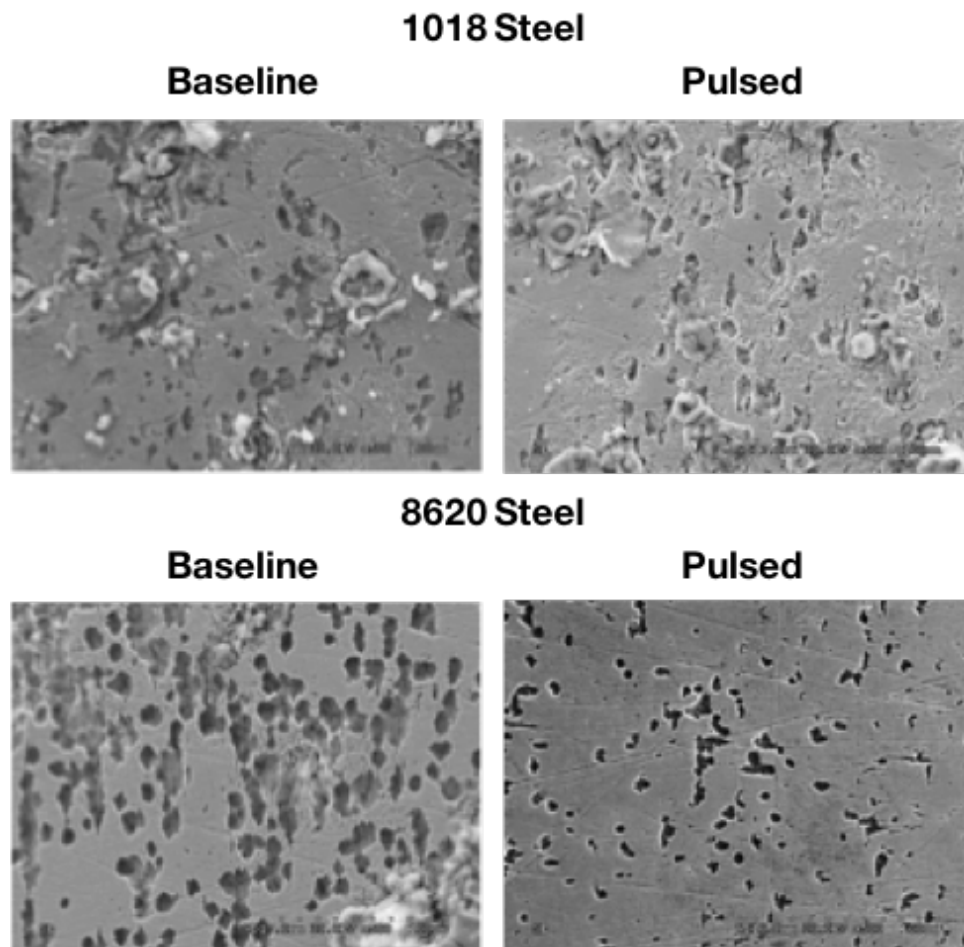
Figure 4-24 SEM images taken of the 1018 steel (top) and 8620 steel (bottom) samples with and without pulsed current in 3.5% NaCl in open air at room temperature

The images taken after each experiment with 1018 steel, shown on top of Figure 4-24, shows that pitting is present on the sample surfaces. After exposure to pulsed currents, the density of pitting remained similar while the width of the pits is increased, when compared with the width of the baseline experiments. This correlates with the results of the linear polarization experiments. The images taken of the 8620 samples, shown in the lower portion of Figure 4-24, reveal an opposite effect after exposure to the pulsed magnetic fields. The pitting density is decreased and the width of the pits is decreased. This again corresponds with the linear polarization results, where the resistance increased after the applied current.

The SEM images taken of the 304 stainless steel and 416 stainless steel samples respectively, are shown in Figure 4-25. The images of the 304 stainless steel sample, shown on top of Figure 4-25, indicate that that there is a reduction in the pitting density after the sample has been exposed to pulsed magnetic fields. It is also evident that the width of the pits is smaller when compared with the baseline sample. Because 304 stainless steel is a corrosive resistant material, the number of pits is low as expected. In the bottom of Figure 4-25, the 416 stainless steel SEM images are presented. Pulsed current appears to have no impact on the pitting density when compared to the baseline sample. Although the density was unaffected, the width of the pits appears to have increased, which is expected since the corrosion resistance decreased after exposure to the pulsed currents.
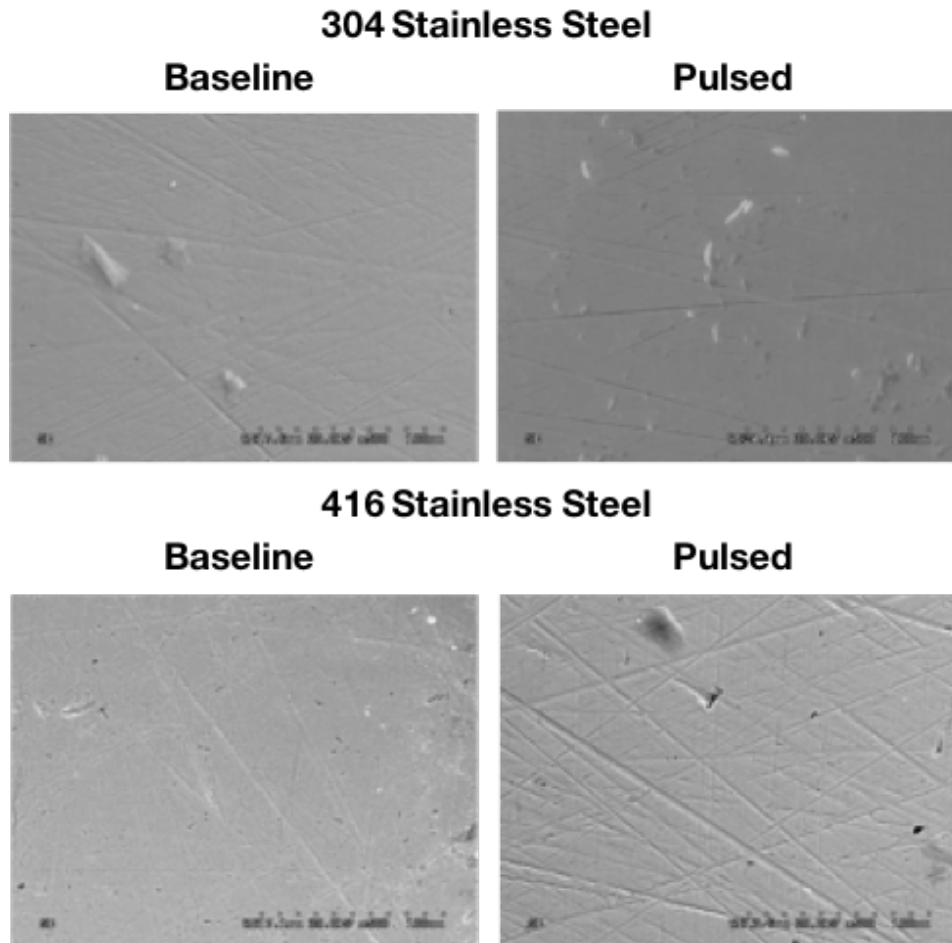
Figure 4-25 SEM taken of the 304 stainless steel (top) and 416 stainless steel (bottom) with and without pulsed current in 3.5% NaCl in open air at room temperature

Surface Characterization of Subjected to a Repeated Pulsed Current while in a Salt Fog

The experiments presented so far have shown that magnetic fields, both externally applied and current-induced, have an effect on the corrosion properties of a few metallic alloys while they are submersed in a 3.5% NaCl electrolyte. This next series of experiments were performed to measure

changes in the corrosion properties when the same four metals, 1018 steel, 8620 steel, 304 stainless steel, and 416 stainless steel, were pulsed with current while they were exposed to a salt fog. In this set of experiments, the samples were subjected to ten pulses at a rate of one pulse per minute. The repetition rate was increased so that a higher average temperature would be maintained. In each experiment, the pulsed discharge was applied with the pulsed power supply charged to 100 V while each of the following nine pulses were applied from the power supply initially charged to only 75 V. The initial higher charge was to get a faster rate of thermal rise while each of the next nine was intended to maintain the temperature at an average temperature close to 60°C. The sample was exposed to a salt fog for one hour. After the one-hour period was completed, the ten pulses were applied with the salt fog still present, and finally the sample was rested in the salt fog for one additional hour before being characterized. Samples not pulsed were current were also studied but instead of being pulsed during the ten-minute period, they rested ten minutes in the salt fog.

SEM images taken of the 1018 steel samples are shown in Figure 4-26 through Figure 4-28. It should be noted that multiple images were taken of each sample at each stage of experimentation. Those shown are representative of the majority of images taken and only these are shown in the interest of page count. Figure 4-26, shows the SEM image of a prepared 1018 steel sample that is representative of the both samples before the pulsed and baseline

experiments were performed. An SEM image of the sample subjected to both the repeated pulsed currents and a salt fog is shown in Figure 4-27. The surface of this sample has started to pit and oxidation growth has formed on the surface. A few salt crystals can be seen on the surface but they are relatively small compared to the oxide growth. An SEM photograph of the baseline 1018 sample, after it was exposed to two hours and ten minutes of salt fog, is shown in Figure 4-28. When compared to the pulsed sample, there is a larger amount of oxidation growth. This indicates that the application of pulsed current appears to reduce the development of an oxide and increases the size of the pits formed in the 1018 steel.
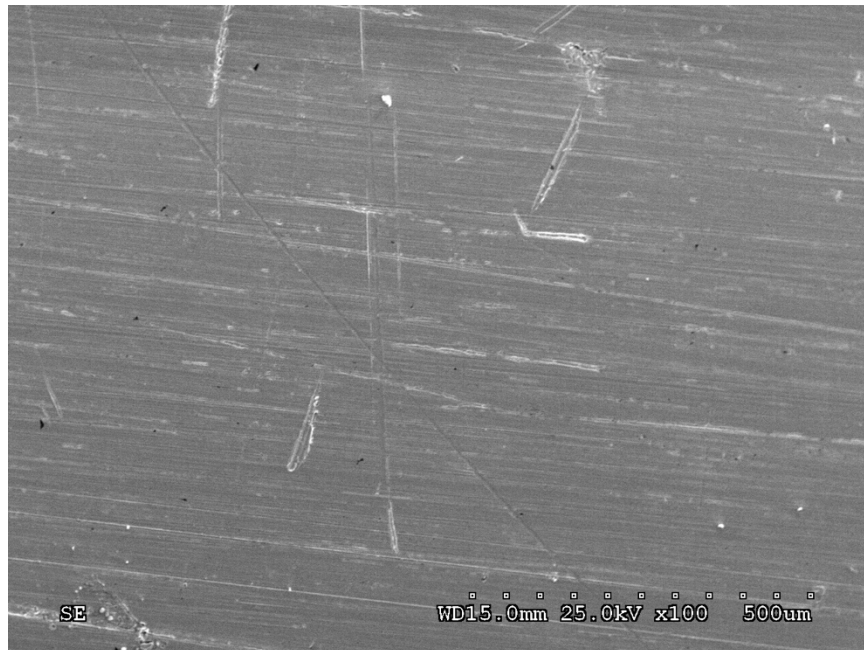
Figure 4-26 SEM image of a prepared 1018 steel sample

Figure 4-27 SEM image of a 1018 steel sample subjected to both the pulsed current and salt

fog
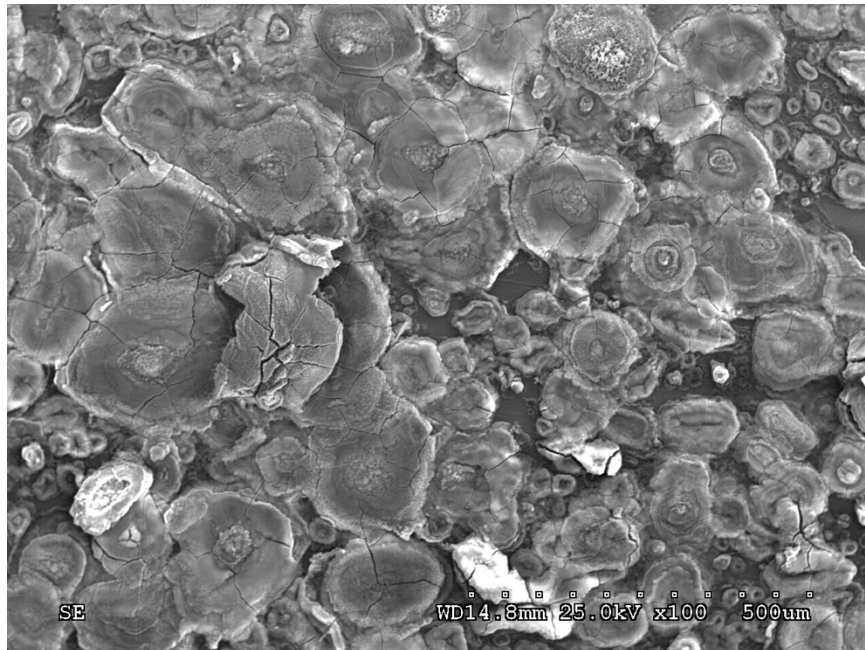
Figure 4-28 SEM image of 1018 steel sample subjected to only a salt fog

Table 6 shows the elemental weight percentages, obtained using EDS measurements, of the baseline and pulsed 1018 samples after the experiments had been performed. As seen in the table, the pulsed sample has less oxygen on the surface than the baseline salt fog sample. This aligns with the conclusions drawn from the SEM images where more oxide is seen on the baseline salt fog sample. The EDS results also show a higher percentage of Na and Cl on the surface of the baseline salt fog sample as compared to the pulsed sample.

Table 6 EDS weight percentages of the prepared, pulsed, and salt fog 1018 steel sample

	C (%)	Fe (%)	MN (%)	Na (%)	Cl (%)	O (%)	Other (%)
Prepared Sample	3.03	95.29	0.93	0.00	0.00	0.00	0.75
Pulsed Sample	4.25	76.17	0.75	0.31	0.22	17.84	0.45
Salt Fog Sample	2.23	66.68	0.70	0.87	0.34	28.96	0.21

SEM images of the two respective 8620 steel samples are shown in Figure 4-29 through Figure 4-31. Figure 4-29 presents an image of a prepared sample that represents the 8620 steel samples before any experiments were performed. Figure 4-30 displays an image of the 8620 steel sample that was subjected to repeated pulsed current flow within a salt fog. The image shows that there is a higher level of oxidation on the surface of this sample than there was on the 1018 steel sample. This is likely attributed to the chromium content in the 8620 steel that is not in the 1018 steel.

Figure 4-29 SEM image of the prepared 8620 steel sample
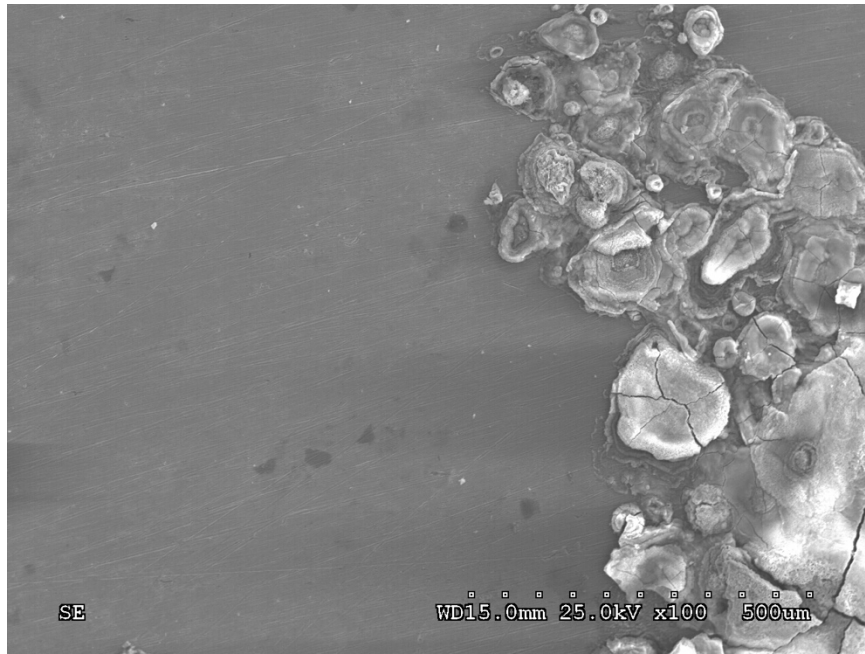

Figure 4-30 SEM image of the 8620 steel sample subjected to both the pulsed current and salt

fog
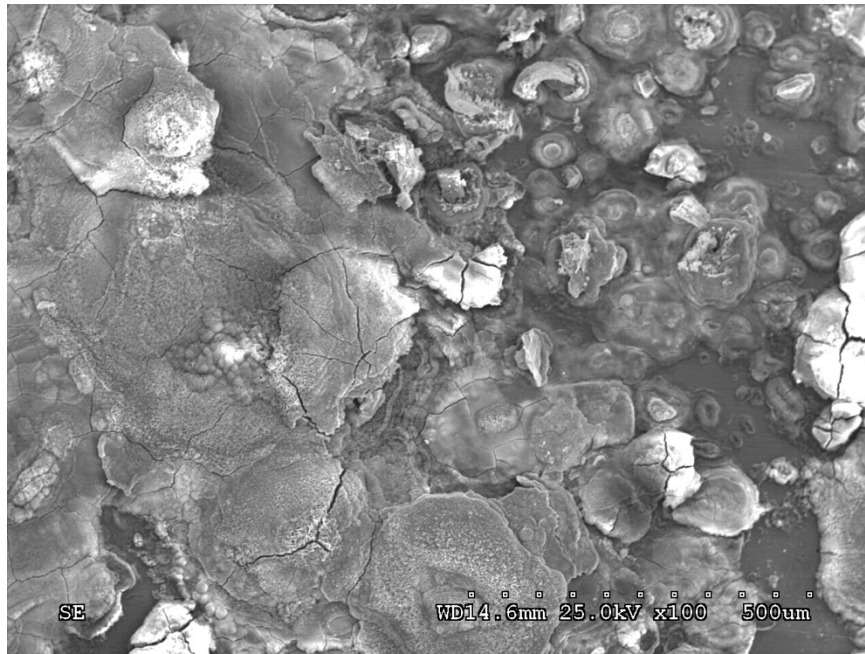
Figure 4-31 SEM image of the 8620 steel sample subjected to only the salt fog

With the increased level of oxidation, the amount of pitting on the surface was decreased as compared to that seen on the 1018 steel sample. The oxidation growth appears to be less developed on the pulsed sample than it does on the sample than it does on the baseline salt fog sample, shown in Figure 4-31. The EDS results obtained when the 8620 steel sample was analyzed is presented in

Table 7. From the results, it is seen that the weight of oxygen is roughly the same on both the pulsed and baseline salt fog samples, which agrees with the conclusions drawn from the SEM images. The variation in the oxidation formation may be contributed to the quick changes in oxygen concentration effectively change reaction rates with every current pulse. The weights of sodium and chlorine on each respective sample are also similar. From these

results it can be concluded that the conduction of repeated pulsed currents has less impact on 8620 steel than the 1018 sample. It is hypothesized that the small amount of chromium in 8620 steel is reacting quick enough with the oxygen to form an oxide layer before pitting.

Table 7 EDS weight percentages of the prepared, pulsed, and salt fog 8620 steel sample

	C (%)	Fe (%)	MN (%)	Cr (%)	Ni (%)	Na (%)	Cl (%)	O (%)	Other (%)
Prepared Sample	3.92	91.25	1.10	0.59	0.59	0.00	0.00	0.00	2.55
Pulsed Sample	4.48	59.19	0.72	0.25	0.39	0.57	1.24	32.82	0.34
Salt Fog Sample	4.58	58.74	0.66	0.20	0.25	0.59	0.87	34.06	0.05

SEM images of the 304 stainless steel samples are shown in Figure 4-32 through Figure 4-34. The prepared 304 stainless steel sample is shown in Figure 4-32 and this image is representative of all the samples before they were subjected any form of experimentation. The 304 stainless steel sample that carried the repetitive pulsed currents is shown in Figure 4-33. The image shows a large amount of pitting on the surface of the sample. There is a small amount of oxide growth that has developed on the sample but it is minimal as compared to the two steel samples presented earlier. The sample subjected to only the salt fog is shown in Figure 4-34 and there does not appear to be any evidence of pitting on the surface. The pitting corrosion may be a result of the sudden increase in oxygen concentration affecting the potential of the sample and putting it in the transpassive region effectively pitting the entire surface.   In this particular image, there is a salt crystal that remained on the surface.

Figure 4-32 SEM image of the prepared 304 stainless steel sample

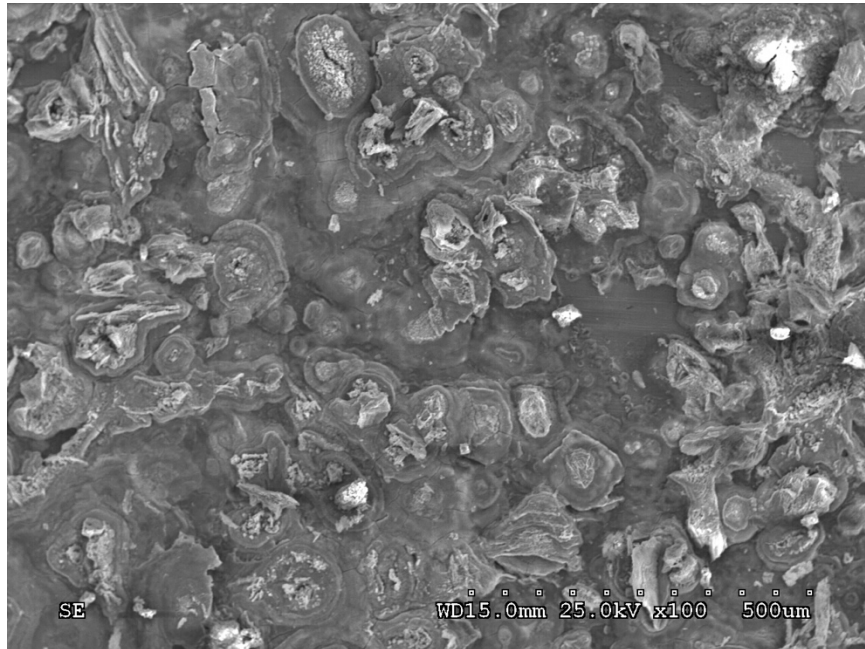

Figure 4-33 SEM image of the 304 stainless steel sample subjected to both the pulsed current

and salt fog
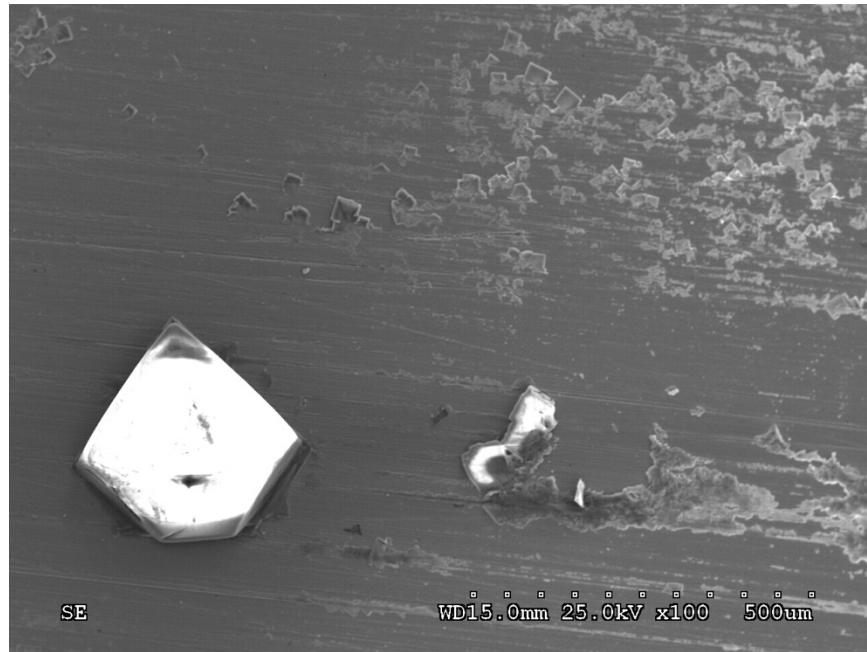
Figure 4-34 SEM image of the 304 stainless steel sample subjected to only the salt fog

This would accelerate future corrosion products as it would increase ion flow in any solution it would mix with. The salt crystal may be a result of the stainless steel samples reaching over 100°C, which evaporated the solution quickly reducing the salt on the surface.

Table 8 presents the EDS results obtained for all of the 304 stainless steel samples. It should be noticed from comparison of this table to those presented earlier that 304 stainless steel has the highest chromium content of the four alloys tested. Sodium and chlorine concentration was highest on the baseline salt fog only sample. From all of the images taken, there was no evidence of oxygen on the surface of the baseline salt fog sample however there is evidence of oxidation on the sample that carried high pulsed currents.

Stainless steel in open air is already in a very stable form. It would require a higher than normal oxygen concentration to begin the corrosion reactions. This case occurs when the sample is pulsed as it draws oxygen to the surface. It appears that the conduction of repeated pulsed currents decreases the sodium and chlorine concentration, but increased the oxygen concentration. It is believed the higher temperature is lowering the salt crystals while the self-induced magnetic field is increasing the oxygen concentration.

Table 8 EDS weight percentages of the prepared, pulsed, and salt fog 304 stainless steel sample

	C (%)	Fe (%)	MN (%)	Cr (%)	Ni (%)	Na (%)	Cl (%)	O (%)	Other (%)
Prepared Sample	4.15	66.67	2.20	18.11	7.15	0.00	0.00	0.00	1.72
Pulsed Sample	7.57	59.61	2.03	16.39	6.17	3.89	1.15	2.38	0.82
Salt Fog Sample	2.38	55.24	1.81	15.50	5.68	13.38	5.29	0.00	0.72

The last alloy experimentally evaluated was 416 stainless steel. The SEM images taken of those samples are shown in Figure 4-35 through Figure 4-37. Figure 4-35 shows an image taken of a prepared 416 stainless steel sample before any experiments were performed. From Figure 4-36, it should be observed that there is less pitting on the surface of the 416 stainless steel sample that was pulsed with current than there is on the 304 stainless steel sample that was pulsed. Again, this pitting is thought to be from an increase in oxygen concentration putting the sample in the transpassive region.
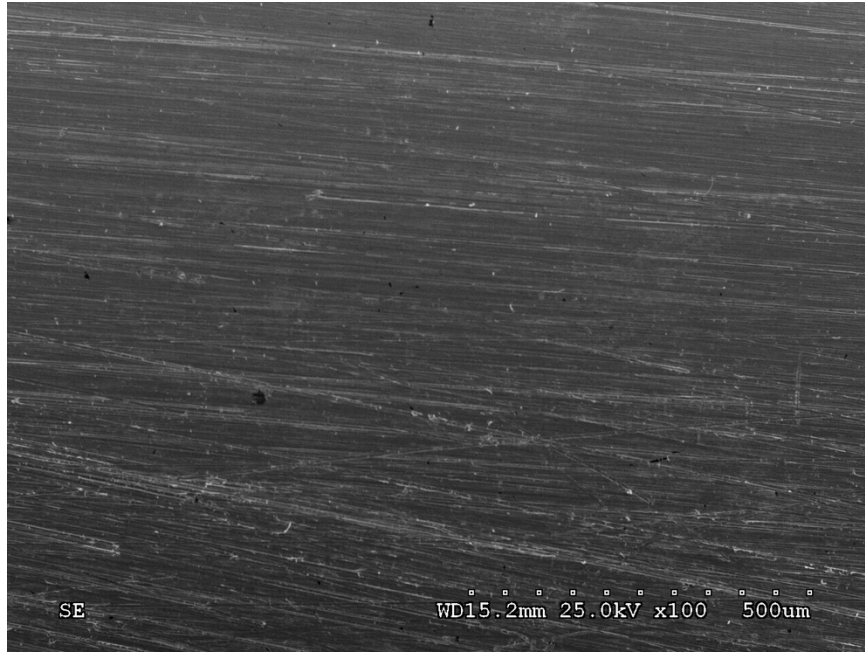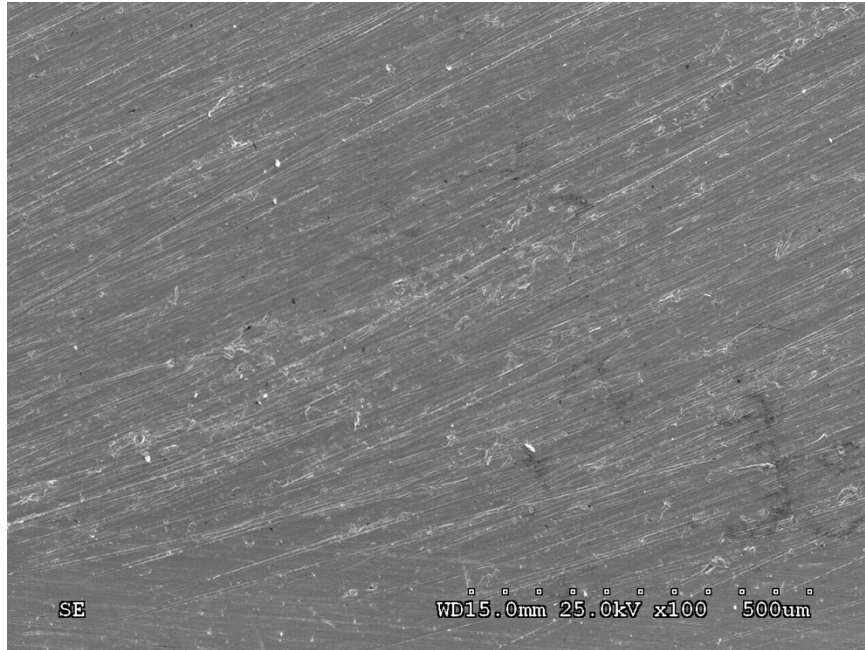
Figure 4-35 SEM image of the prepared 416 stainless steel sample
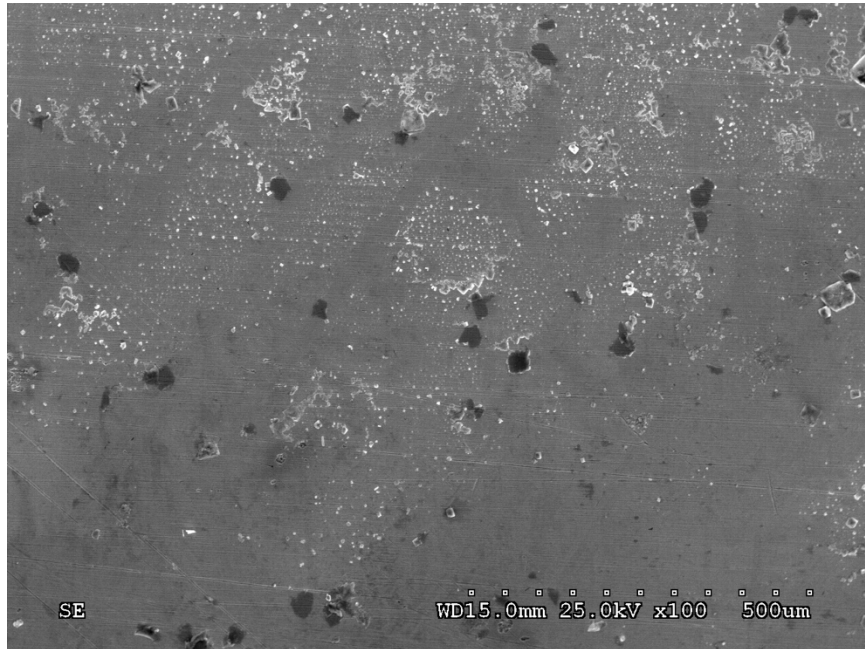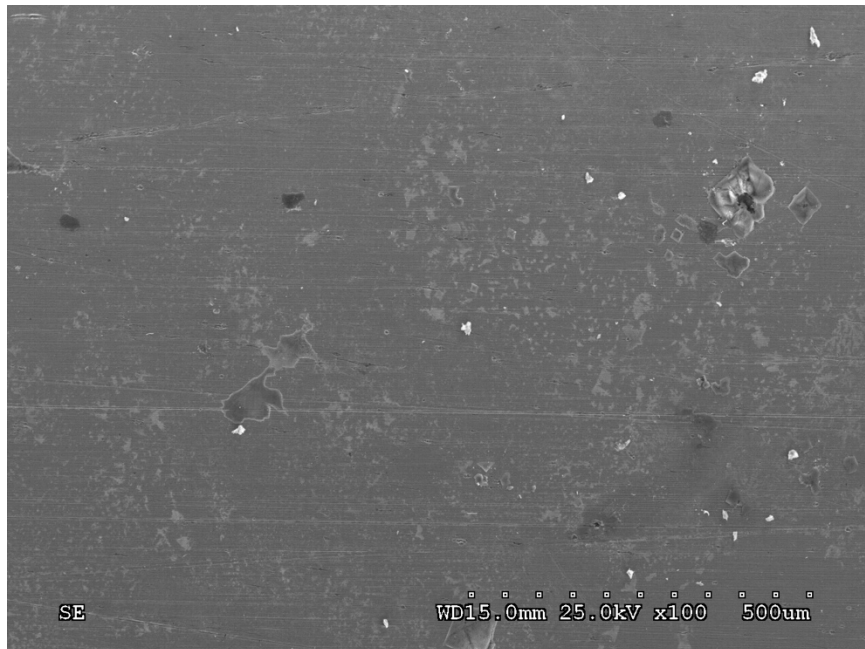

Figure 4-36 SEM image of the 416 stainless steel sample subjected to both the pulsed current

and salt fog
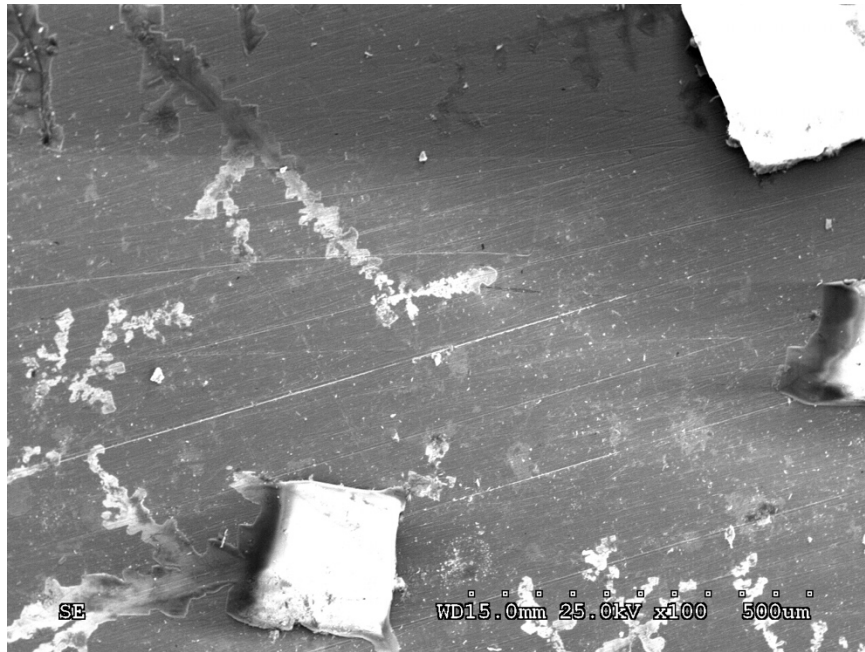
Figure 4-37 SEM image of the 416 stainless steel sample subjected to only the salt fog

In this image, it appears that there is some oxide growth but it is rather small.

The 416 stainless steel baseline salt fog sample is shown in Figure 4-37 where

there is heavier formation of an oxide on the surface. Similar to the results for

the 304 stainless steel baseline salt fog sample, there are large NaCl crystals

present on the surface. As mentioned before, the salt crystal deposits are

reduced on the pulsed sample as the samples is evaporating the solution on the

surface.

The EDS results obtained from the 416 stainless steel samples are

presented in Table 9. Similar to the 304 stainless steel samples, the sodium

and chlorine percentages are highest on the baseline salt fog sample. The

oxygen percentage is also highest on the pulsed sample. This may be

contributed to the increased oxygen concentration at the surface of the sample from the self-induced magnetic field.

Table 9 EDS weight percentages of the prepared, pulsed, and salt fog 416 stainless steel sample

	C (%)	Fe (%)	MN (%)	Cr (%)	Na (%)	Cl (%)	O (%)	Other (%)
Prepared Sample	3.86	80.93	1.44	12.38	0.00	0.00	0.00	1.39
Pulsed Sample	5.05	73.56	1.20	11.61	4.68	1.44	1.36	1.10
Salt Fog Sample	3.23	67.39	1.13	10.83	11.62	4.22	0.27	1.31

Chapter 5 Summary and Conclusion

The research documented in this dissertation was performed with the aim of more fundamentally understanding how high magnetic fields affect a metallic alloys rate of corrosion. The US Navy has a long term goal of transitioning to a more electric fleet. As they do this, the amount of electrical generation aboard the ship will increase significantly and the number of loads will increase as well. Many of the loads will demand energy in similar fashion to those historically aboard naval vessels while others will demand incredibly power in a more transient manner. Especially in the latter types of loads, there will be high magnetic fields generated. The metals carrying the current from the source to the load will be exposed to these high magnetic fields and so too will many structural materials that are located in close proximity to the conductors and loads. Since naval vessels will nearly always be in a highly corrosive environment, there are questions about how the high magnetic fields will impact the corrosive properties of both the conductors and structural alloys on board a ship, leading the work proposed here. It is critical that the US Navy understand these relationships before high magnetic fields are operated aboard the next generation of electric vessels.

Prior to this work, there were several published reports that documented the relationship between continuous magnetic fields and the corrosion of a few different metallic alloys [16] [17] [18] [19] [20]. Though these reports were useful, the magnetic fields experimentally applied were quite low and none of

them documented the impact of pulsed current carry, and the magnetic fields induced by the conduction of pulsed currents, on the corrosive properties. In the work presented here, the impact of both continuous magnetic fields as high 0.45 T and current induced magnetic fields in excess of a few T have been presented. The results have shown that magnetic fields do have an effect on the way metallic alloys corrode.

A number of unique sets of experiments were presented in the work discussed here. In the first, the corrosion potential of four metallic alloys including 1018 steel, 8620 steel, 304 stainless steel, and 416 stainless steel were measured both inside and outside of a 0.45 T magnetic field. The magnetic field was generated using an electromagnet and the results showed that the magnetic field strongly influenced the corrosion potential. It was shown that that a metallic alloy with ferromagnetic properties was more strongly affected since the magnetic field is non-uniform across the samples surface. The outer edges feel a stronger metallic gradient. It was hypothesized that the change in the corrosion potential was a result of a change in the concentration of oxygen across the samples surface. The concentration is changed due to oxygen's paramagnetic nature which causes it to align with the magnetic fields, increasing its density at the samples edges where the fields are stronger. 304 stainless steel, which has no ferromagnetic properties, was affected the least as opposed to the other three materials which have ferromagnetic properties.

In the second set of experiments, the earlier hypothesis speculating that magnetic fields affect the concentration of oxygen on the sample's surface was proven correct when the same sets of experiments were performed, but this time with the oxygen in the electrolyte displaced by argon. It was shown that when all of the ferromagnetic materials were studied, the corrosion potential only shifted when oxygen was present in the electrolyte. When argon was present in place of oxygen, there was no shift in the corrosion potential when magnetic fields were applied. This was a new and novel contribution to the field as this has never been demonstrated before.

In the third set of experiments, the same four metallic alloys were studied and additional alloys, including C11000 copper, C18200 copper, 6061-T6 aluminum, and 7075-T6, were studied and anodic polarization measurements were studied. From those measurements, each alloy's corrosion regions were studied and it was found that the ferromagnetic alloys saw larger changes in their corrosion properties compared to the diamagnetic materials. Both aluminum alloys have a small amount of iron concentration, which is the reason the aluminum alloys saw more dramatic changes than the two copper alloys. When exposed to an external magnetic field it can be determined if the corrosion properties will be effected by determining if the alloy is ferromagnetic. The degree of change to the corrosion properties can be determined by evaluating the permeability of the alloy. A higher permeability will result in larger changes in the corrosion properties.

Finally, a host of experiments were performed in which 1018 steel, 8620 steel, 304 stainless steel, and 416 stainless steel rod samples were pulsed with repetitive high pulsed currents to study the affect that current flow and self-induced magnetic fields has on the corrosive properties of the alloys. Using SEM imaging, EDS composition measurements, and linear polarization measurements, it was shown that the conduction of pulsed currents does have an impact on the way each metal corrodes. When samples that were pulsed were compared with samples that were not pulsed, but still exposed to an electrolyte, it was shown that the pitting density and amount of oxidation on each type of sample was affected by the self-induced magnetic field. All of the alloys tested were affected by the self-induced magnetic field regardless of the alloys ferromagnetic properties. The effect from the magnetic field was uniform across the surface of the alloy because the flux density of the magnetic field was uniform on the surface of the sample. A main concern of alloys subjected to pulsed currents is increase in the pitting corrosion, which can severely degrade an alloy with no visual indication of it occurring.

In conclusion, it has been shown that high magnetic fields do strongly affect the way a metal corrodes. The two most important conclusions are that oxygen is more heavily drawn to the surface of a ferromagnetic alloys, increasing the rate of corrosion or passivation, and that the conduction of high pulsed currents has an impact on the pitting and oxidation growth on the surface. Though there are no strong recommendations on how future engineers

118

should respond to these conclusions when designing future ships, they are important findings that should be considered. It is greatly hoped that this work is useful to future shipboard electrical system engineers and that this work can be a basis for future work. In conclusion, a few of these findings are summarized in bullet form below.

Bulleted Summary of Findings

- Ferromagnetic properties of an alloy dictate the amount of change to the corrosion properties when exposed to an external magnetic field

- A self-induced magnetic field produced from pulsed current will affect all alloys regardless of their ferromagnetic properties

- The time between current pulses effects the amount of oxidation and pitting growth on the surface

- An alloy subjected to a pulsed current will see reduced salt crystal formation on the surface after being subjected to a NaCl solution

- The magnetic field is influencing the corrosion properties of an alloy by redistributing the oxygen concentration at the surface of the sample

Works Cited

[1] M. Nakagawa and et al., "Effects of Fluoride and Dissolved Oxygen Concentrations on the Corrosion Behavior of Pure Titanium and Titanium Alloys," *Dental Materials Journal,* vol. 21, no. 2, pp. 83-92, March 2002.

[2] D. Smith and B. McEnaney, "The Influence of Dissolved Oxygen Concentration on the Corrosion of Grey Cast Iron in Water at 50C," *Corrosion Science,* vol. 19, no. 6, pp. 391-389-394, November 1978.

[3] S. Littlefield and A. Nickens, "Roadmap for the all-electric Warship," Power, 15 February 2005. [Online]. Available: http://www.powermag.com/roadmap-for-the-all-electric-warship/?pagenum=1. [Accessed 4 April 2016].

[4] M. Nafar and et al., "Magnetic Field Calaculation of 63kV Transmission Lines," *IJRRAS,* vol. 17, no. 2, pp. 218-224, November 2013.

[5] M. Abdel-Salam and et al., "Calculation of Magnetic Fields from Electric Power Transmission Lines," *Electric Power Systems Research,* vol. 49, no. 2, pp. 99-105, March 1999.

[6] D. P. Stern, "Magnetism," 25 November 2001. [Online]. Available: http://www-istp.gsfc.nasa.gov/Education/Imagnet.html. [Accessed 25 August 2016].

[7] "Diamagnetic, Paramagnetic, and Ferromagnetic MAterials," NDT resource Center, [Online]. Available: https://www.nde-ed.org/EducationResources/CommunityCollege/MagParticle/Physics/MagneticMatls.htm. [Accessed 25 August 2016].

[8] J. C. Maxwell, A treatise on electricity and magnetism, vol. 1, Oxford: Macmillan and co. .

[9] C. R. Nave, "HyperPhysics," [Online]. Available: http://hyperphysics.phy-astr.gsu.edu/hbase/forces/funfor.html. [Accessed 25 August 2016].

[10] R. Kurtus, "Moving Electrical Charges Create Magnetic Fields," School for Champions, 23 March 2012. [Online]. Available: http://www.school-for-champions.com/science/magnetic_field_moving_charges.htm#.V78RDWXQ70c. [Accessed 25 August 2016].

[11] "How does rust work?," How Stuff Works, [Online]. Available: http://science.howstuffworks.com/question445.htm. [Accessed 25 August 2016].

[12] "Galvanic Corrosion," NACE International , [Online]. Available: https://www.nace.org/Corrosion-Central/Corrosion-101/Galvanic-Corrosion/. [Accessed 25 Aug 2016].

[13] M. Blaber, "Electrochemisty Voltaic Cells," 10 May 2000. [Online]. Available: http://www.mikeblaber.org/oldwine/chm1046/notes/Electro/Voltaic/Voltaic.htm. [Accessed 1 June 2016].

[14] D. Kopeliovich, "Galvanic corrosion," SubsTech, 21 7 2015. [Online]. Available: http://www.substech.com/dokuwiki/doku.php?id=galvanic_corrosion. [Accessed 1 June 2016].

[15] D. Kopeliovich, "Pitting Corrosion," SubsTech, 21 July 2015. [Online]. Available: http://www.substech.com/dokuwiki/doku.php?id=pitting_corrosion. [Accessed 4 June 2016].

[16] P. Linhardt and et al., "Electrochemical investigation of chloride induced pitting of stainless steel under the influence of a magnetic field," *Corrosion Science,* vol. 47, no. 7, pp. 1599-1603, 2005.

[17] P. Linhardt and et al., "Pitting of stainless steel under the influence of a magnetic field," 27 December 2012. [Online]. Available: http://info.tuwien.ac.at/cta/korrosion/forschung/magnet.html. [Accessed 14 May 2014].

[18] P. Linhardt and et al., "Electrochemical investigation of chloride induced pitting of stainless steel under the influence of a magnetic field," in *4th Kurt Schwabe Symposium Mechanisms of Corrosion and Corrosion Prevention*, Finland, 2004.

[19] A. Sato and et al., "Influence of high magnetic field on the corrosion of carbon steel," *Applied Superconductivity, IEEE Transactions on. ,* vol. 12, no. 1, pp. 997-1000, 2002.

[20] M. A. Ghabashy, "Effect of magnetic field on the rate of steel corrosion in aqueous solutions," *Anti-Corrosion Methods and Materials,* vol. 35, no. 1, pp. 12-13, 1988.

[21] R. Pietrzak and R. Szatanik, "Effect of magnetic field on the corrosion of iron as studied by positron annihilation," *Nukleonika,* vol. 55, no. 1, pp. 31-34, 2010.

[22] J. Hu and et al., "Effects of Applied Magnetic Field on Corrosion of Beryllium Copper in NaCl Solution," *J. Mater. Sci. Technol.,* vol. 26, no. 4, pp. 355-361, 2010.

[23] N. Hirota and et al., "Rise and Fall of Surface Level of Water Solutions under High Magnetic Fields," *Japanese Journal of Applied Physics,* vol. 34, no. 2, pp. 991-993, August 1995.

[24] Z. Chen and E. D. Dahlberg, "Deformation of Water by a Magnetic Field,"

The Physics Teacher, vol. 49, pp. 144-146, 2011.

[25] S. Ueno and K. Harada, "Redistribution of Dissolved Oxygen Conventration Under Strong DC Magnetic Fields," *IEEE Transactions on Magnetics,* vol. 18, no. 6, pp. 1704-1706, November 1982.

[26] S. Ueno and M. Iwaska, "Properties of Magnetic Curtain Produced by Magnetic Fields," *J. Appl. Phys. ,* vol. 67, no. 9, pp. 5901-5903, May 1990.

[27] S. Ueno, M. Iwasaka and T. Kitajima, "Redistribution of Dissolved Oxygen Concentration under Magnetic Fields up to 8 T," *Journal of Applied Physics,* vol. 75, no. 10, pp. 7174-7176, May 1994.

[28] L. Ji-nan and et al., "Effects of Rotating Electromagnetic on Flow Corrosion of Copper in Seawater," *Transaction of Nonferrous Metals,* vol. 21, no. 2, pp. 489-493, July 2011.

[29] N. M. Yakupov and et al., "Effect of a Magnetic Field on Corrosive Wear," *Doklady Physics,* vol. 57, no. 3, pp. 104-106, 2012.

[30] B. Wang and et al. , "Effects of Pulse Electromagnetic Field on Corrosion Resistance of Al-5 % Cu Alloy," *J Low Temp Phys,* vol. 170, no. 5, pp. 418-423, August 2012.

[31] J. C. Sanchez-Ghenno and et al., "Effects of Magnetic FIelds on the Corrosion Behavior of Hyrdocarbon Transmission Pipelines," in *NACE international ,* San Antonio, 2010.

[32] R. Sueptitz and et al., "Impact of Magnetic Field Gradients on the Free Corrosion of Iron," *Electrochimica Acta,* vol. 55, no. 18, pp. 5200-5203, July 2010.

[33] X. Zhang and et al., "Magnetic-Field-Induced Microstructural Features in a High Carbon Steel during Diffusional Phase Transformation," *Journal of Magnetism and Magnetic Materials ,* vol. 324, no. 24, pp. 4184-4188, July 2012 .

[34] B. Beverskog and I. Puigdomenech, "Revised Pourbaix diagrams for iron at 25-300 C," *Corrosion Science,* vol. 38, no. 12, pp. 2121-2135, 1996.

[35] G. Grieder, "Left Hand Rule," Tangient, 13 June 2012. [Online]. Available: https://physick.wikispaces.com/Left+Hand+Rule. [Accessed 5 April 2016].

Biographical Information

Clint Gnegy-Davidson was born in Bedford, Texas in 1991. He received a B.S. degree in electrical engineering in 2013 from the University of Texas at Arlington with highest honors as summa cum laude. He was a member and officer of many student organizations including IEEE, HKN, and ANS. He spent a summer interning at the Naval Surface Warfare Center Dahlgren in Virginia. His research includes electro-chemistry, power electronics, pulsed power, directed energy, and energy storage.